

NUMERICAL SIMULATION STUDIES OF
THE EFFECT OF MEMBRANE PERMEANCE
ON MASS TRANSFER ENHANCEMENT
DRIVEN BY TRANSIENT SLIP VELOCITY



LIM SOON YEE

اونيورسيتي مليسيا قهغ

UNIVERSITI MALAYSIA PAHANG

MASTER OF SCIENCE

UNIVERSITI MALAYSIA PAHANG

UNIVERSITI MALAYSIA PAHANG

DECLARATION OF THESIS AND COPYRIGHT

Author's Full Name : LIM SOON YEE

Date of Birth : 13/12/1991

Title : NUMERICAL SIMULATION STUDIES OF THE
EFFECT OF MEMBRANE PERMEANCE ON MASS
TRANSFER ENHANCEMENT DRIVEN BY TRANSIENT
SLIP VELOCITY

Academic Session : SEMS I 2020/2021

I declare that this thesis is classified as:

- CONFIDENTIAL (Contains confidential information under the Official Secret Act 1997)*
- RESTRICTED (Contains restricted information as specified by the organization where research was done)*
- OPEN ACCESS I agree that my thesis to be published as online open access (Full Text)

I acknowledge that Universiti Malaysia Pahang reserves the following rights:

1. The Thesis is the Property of Universiti Malaysia Pahang
2. The Library of Universiti Malaysia Pahang has the right to make copies of the thesis for the purpose of research only.
3. The Library has the right to make copies of the thesis for academic exchange.

Certified by:

(Student's Signature)

911213045200

New IC/Passport Number
Date:

(Supervisor's Signature)

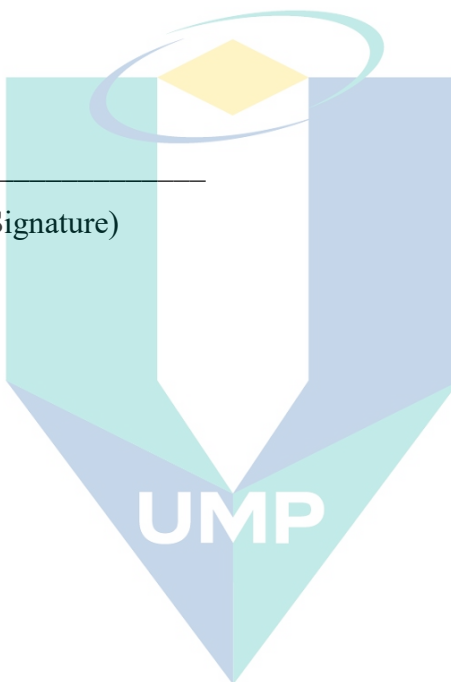
Name of Supervisor
Date:

NOTE : * If the thesis is CONFIDENTIAL or RESTRICTED, please attach a thesis declaration letter.



SUPERVISOR'S DECLARATION

I hereby declare that I have checked this thesis and in my opinion, this thesis is adequate in terms of scope and quality for the award of the degree of Master of Science.



(Supervisor's Signature)

Full Name :
Position :
Date :

اونيورسيتي ملايسيا قهغ

UNIVERSITI MALAYSIA PAHANG

STUDENT'S DECLARATION

I hereby declare that the work in this thesis is based on my original work except for quotations and citations which have been duly acknowledged. I also declare that it has not been previously or concurrently submitted for any other degree at Universiti Malaysia Pahang or any other institutions.

(Student's Signature)

Full Name : LIM SOON YEE

ID Number : MKC16015

Date :

اونیورسیتی ملیسیا قهغ

UNIVERSITI MALAYSIA PAHANG

NUMERICAL SIMULATION STUDIES OF THE EFFECT OF MEMBRANE
PERMEANCE ON MASS TRANSFER ENHANCEMENT DRIVEN BY
TRANSIENT SLIP VELOCITY



Thesis submitted in fulfillment of the requirements
for the award of the degree of
Master of Science

اونيورسيتي ملايسيا قهغ

UNIVERSITI MALAYSIA PAHANG

Faculty of Chemical and Process Engineering Technology

UNIVERSITI MALAYSIA PAHANG

NOVEMBER 2020

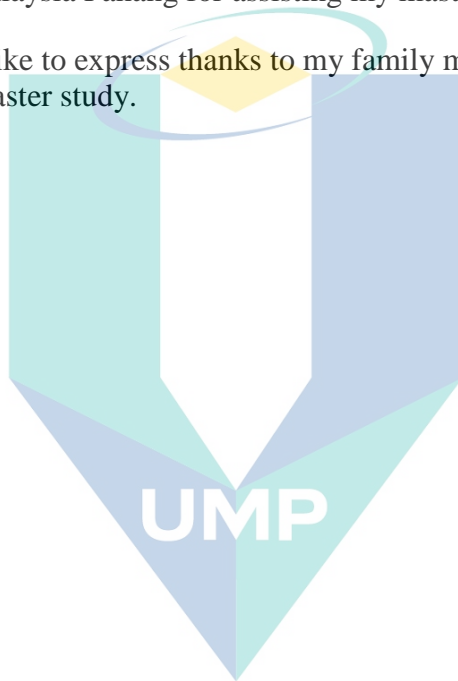
ACKNOWLEDGEMENTS

First, I would like to thank my supervisor, Dr Liang Yong Yeow for his guidance to complete this thesis.

I would also like to show my appreciation to the staff of Faculty of Chemical and Process Engineering Technology of Universiti Malaysia Pahang for technical support.

I also wish to thank the help provided by the staff of the Institute of Postgraduate Studies (IPS) of Universiti Malaysia Pahang for assisting my master studies.

Finally, I would also like to express thanks to my family members who have encouraged me to complete my master study.



اونيورسيتي مليسيا قهغ

UNIVERSITI MALAYSIA PAHANG

ABSTRAK

Salah satu pencapaian yang paling penting dalam kecekapan osmosis (RO) berbalik adalah peningkatan dalam membran kadar resapan. Walaupun membran semasa menawarkan kadar resapan yang lebih tinggi (dan fluks) daripada membran RO terdahulu, peningkatan fluks dihadkan oleh polarisasi konsentrasi (CP) dan fouling. Oleh itu, inovasi adalah diperlukan untuk mengurangkan polarisasi konsentrasi untuk terus meningkatkan fluks. Halaju slip terpaksa yang tidak stabil dapat mengganggu sempadan lapisan, sekali gus mengurangkan CP. Kajian penyelidikan ini telah mengaplikasikan Pengkomputeran Bendalir Dinamik (CFD) bagi tujuan analisis kesan ketertelapan membran kepada frekuensi optimum untuk halaju slip yang tidak stabil, serta peningkatan pemindahan jisim yang terhasil. Hasil dapatan kajian penyelidikan ini telah menunjukkan bahawa frekuensi optimum halaju slip yang tidak stabil tidak akan terjejas oleh ketertelapan membran. Walaupun hasil dapatan kajian menunjukkan peningkatan dalam faktor penambahan pemindahan jisim untuk nilai ketertelapan dalam julat yang biasanya digunakan untuk air payau, fluks permeate (permeate flux) juga boleh ditingkatkan untuk meningkatkan ketertelapan membran (sehingga 23%) dengan menggunakan tenaga pam yang sedikit lebih tinggi (sehingga 5-7%). Selain itu, tesis ini mendapati bahawa untuk semua ketertelapan membran, halaju slip dapat meningkatkan tegasan ricih maksimum sekurang-kurangnya 130%, sekali gus mengurangkan kesan pengotoran.

The logo of Universiti Malaysia Pahang (UMP) is a stylized shield shape composed of four triangles meeting at the center. The top-left triangle is light blue, the top-right is light green, the bottom-left is a darker blue, and the bottom-right is a darker green. The letters 'UMP' are written in white, bold, sans-serif font across the center of the shield.

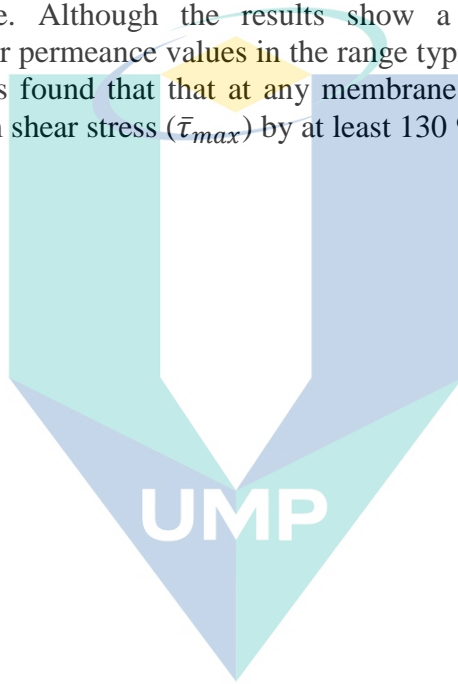
UMP

اونيورسيتي مليسيا قهغ

UNIVERSITI MALAYSIA PAHANG

ABSTRACT

One of the most noteworthy achievements in reverse osmosis (RO) efficiency is the improvement in membrane permeance. Although current membranes offer higher permeance (and flux) than older RO membranes, increases in permeate flux are limited by concentration polarisation (CP) and fouling. Therefore, innovation is needed to reduce CP to further increase permeate flux. An unsteady forced slip velocity can disrupt the boundary layer, thus reducing CP. This paper uses Computational Fluid Dynamics (CFD) to analyse the effect of membrane permeance on the resonant frequency for an unsteady forced slip velocity, as well as the resulting mass transfer enhancement. The results show that the resonant frequency of the unsteady forced slip velocity is not affected by the membrane permeance. Although the results show a peak in the mass transfer enhancement factor for permeance values in the range typically used for brackish water, In addition, this thesis found that that at any membrane permeance, slip velocity can increase the maximum shear stress ($\bar{\tau}_{max}$) by at least 130 %, thus minimising the effects of fouling.



اونيورسيتي ملايسيا قهق

UNIVERSITI MALAYSIA PAHANG

TABLE OF CONTENT

DECLARATION

TITLE PAGE

ACKNOWLEDGEMENTS **ii**

ABSTRAK **iii**

ABSTRACT **iv**

TABLE OF CONTENT **v**

LIST OF TABLES **vii**

LIST OF FIGURES **viii**

LIST OF SYMBOLS **x**

LIST OF ABBREVIATIONS **xii**

CHAPTER 1 INTRODUCTION **1**

1.1 General Overview 1

1.2 Problem Statement 2

1.3 Research Objective 3

1.4 Scope of Study 3

1.5 Novelty of this thesis 4

CHAPTER 2 LITERATURE REVIEW **5**

2.1 Spiral Wound Membrane (SWM) Module 5

2.2 Spacer geometry 7

2.3 Computational Fluid Dynamics (CFD) study of spacer-filled channel 11

2.3.1 Computational Fluid Dynamics (CFD) basics 11

2.3.2 Mesh Independence study 12

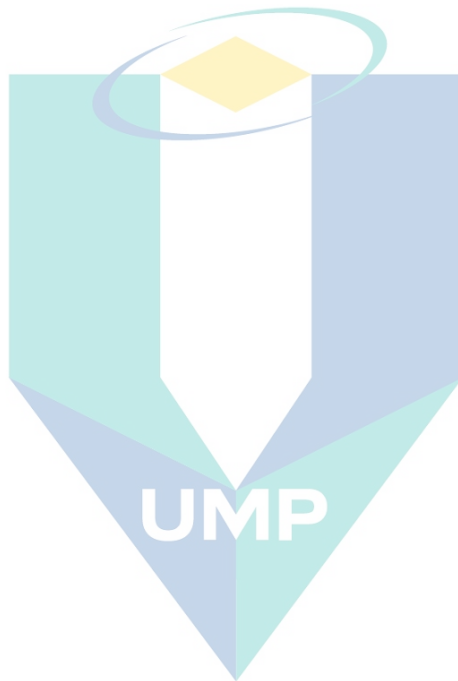
2.4	External techniques for creating flow unsteadiness	14
2.4.1	Vibration method	14
2.4.2	Pulsation method	18
2.4.3	Electro-osmotic flow (EOF) forced slip	20
2.5	Gap analysis	24
CHAPTER 3 METHODOLOGY		25
3.1	Model description	25
3.2	Boundary conditions	28
3.3	Assumption and cases	28
3.4	Methodology for analysis of results	29
CHAPTER 4 RESULTS AND DISCUSSION		33
CHAPTER 5 CONCLUSION AND RECOMMENDATIONS		41
5.1	Conclusions	41
5.2	Recommendations	42
REFERENCES		43

اونیورسیتی ملیسیا قہق

UNIVERSITI MALAYSIA PAHANG

LIST OF TABLES

Table 2.1	Summary of the effect of different perturbation technique	23
Table 3.1	Parameters used for slip velocity case study	27
Table 3.2	Dimensionless variables used for this study	29



اونيورسيتي مليسيا قهغ

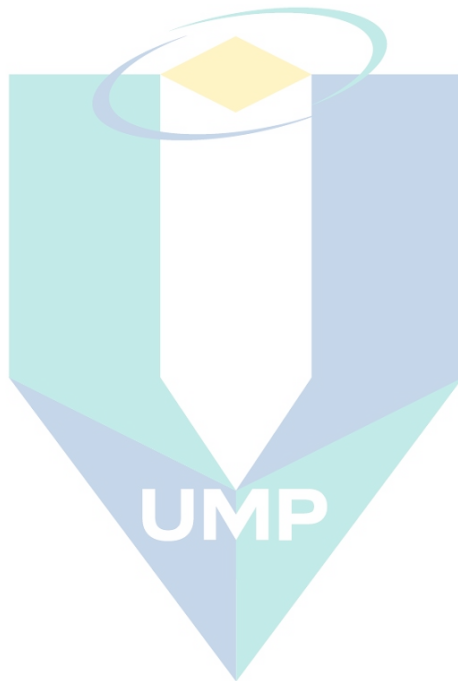
UNIVERSITI MALAYSIA PAHANG

LIST OF FIGURES

Figure 2.1	Types of feed water used (A) for NF/RO around the world and (B) in specific region	5
Figure 2.2	Spiral Wound Membrane (SWM)	6
Figure 2.3	Spacer in SWM modules	8
Figure 2.4	Spacer filament arrangement in a two-dimensional channel	8
Figure 2.5	Rectangular, Cylindrical and triangular spacer	9
Figure 2.6	Velocity vector plot at $Re = 841$. Number 1-8 represents the shed vortices.	11
Figure 2.7	Verification and validation	14
Figure 2.8	Vibration device within desalination cell	17
Figure 2.9	Porous cake layer growth for case without vibration and with vibration	17
Figure 2.10	Velocity profile in the presence and absence of oscillating flow	18
Figure 2.11	Electric double layer structure	21
Figure 3.1	Schematic of fluid domain (not to scale) indicating boundary locations and channel regions. Red arrows on the membrane surface indicate the location of slip velocity	26
Figure 3.2	Geometry of the spacer unit cell	26
Figure 3.3	Flow chart illustrating the steps taken in this study to carry out numerical study to investigate the effect of membrane permeance on permeate flux enhancement generated by unsteady slip velocity.	32
Figure 4.1	Frequency response time data for the pulse slip velocity at monitoring point ‘•’ (located at one third of the channel height from the bottom membrane surface), for $\Pi Lp = 4.94 \times 10^{-5}$, 2.21×10^{-4} , 8.69×10^{-4} and 2.21×10^{-3} at the same feed bulk concentration ($w_{b0} = 0.025$) and $Re = 408$	33
Figure 4.2	Frequency response time data for the corresponding v -velocity at monitoring point ‘•’ (located at one third of the channel height from the bottom membrane surface), for $\Pi Lp = 4.94 \times 10^{-5}$, 2.21×10^{-4} , 8.69×10^{-4} and 2.21×10^{-3} at the same feed bulk concentration ($w_{b0} = 0.025$) and $Re = 408$.	34
Figure 4.3	Frequency response of v -velocity at location ‘•’ to a pulse in slip velocity for $\Pi Lp = 4.94 \times 10^{-5}$, 2.21×10^{-4} , 8.69×10^{-4} and 2.21×10^{-3} at the same feed solute concentration ($w_{b0} = 0.025$) and $Re = 408$	35
Figure 4.4	Effect of membrane permeance on (a) forced slip velocity mass transfer enhancement and (b) relative change in permeate flux at different inlet solute concentration (w_{b0}) of 0.01 ($\Delta p_{tm} = 2.94$ MPa), 0.025 ($\Delta p_{tm} = 2.94$ MPa) and 0.04 ($\Delta p_{tm} = 6$ MPa) for $Re = 408$.	37

Figure 4.5 Effect of slip velocity applied at the F_{peak} on the velocity field and solute concentration in the region within spacer 8 for $\Pi Lp = 4.94 \times 10^{-5}$ and 2.21×10^{-3} at the same feed solute concentration ($w_{b0} = 0.025$) and $Re = 408$. 39

Figure 4.6 Effect of membrane permeance on (a) maximum shear stress and (b) Power number at three different values of w_{b0} : 0.01 ($\Delta p_{tm} = 2.94$ MPa), 0.025 ($\Delta p_{tm} = 2.94$ MPa) and 0.04 ($\Delta p_{tm} = 6$ MPa) for $Re = 408$. 40



اونيورسيتي ملايسيا قهغ

UNIVERSITI MALAYSIA PAHANG

LIST OF SYMBOLS

D	Solute diffusivity ($\text{m}^2 \text{s}^{-1}$)
d_f	Filament diameter (m)
d_h	Hydraulic diameter (m)
E_x	Electric field in the x -direction (V m^{-1})
F_{peak}	Dimensionless actual peak frequency
F_{pl}	Dimensionless peak frequency predicted by frequency response
F_s	Dimensionless frequency of oscillation of slip velocity
f	Friction factor
f_{cut}	Cut-off frequency (s^{-1})
f_s	Frequency of oscillation of slip velocity (s^{-1})
h_{ch}	Height of channel (m)
J	Permeate flux ($\text{kg m}^{-2} \text{s}^{-1}$)
$J_{pure} = \rho L_p \Delta p_{tm}$	Permeate flux through membrane for a pure water system ($\text{kg m}^{-2} \text{s}^{-1}$)
L_{in}	Entrance length (m)
L_m	Membrane length (m)
L_{out}	Exit length (m)
L_p	Membrane permeance ($\text{m s}^{-1} \text{Pa}^{-1}$)
l_m	Mesh length (m)
P_0	Dimensionless inlet transmembrane pressure
P_n	Power number
p	Pressure (Pa)
Δp_{tm}	Inlet transmembrane pressure (Pa)
R	Membrane intrinsic rejection
Re_{CR}	Critical Reynolds number
$Re_h = \frac{\rho u_{eff} d_h}{\mu}$	Hydraulic Reynolds number
Re_s	Slip Reynolds number
t	Time (s)
$U_{s,A}$	Dimensionless forced slip velocity amplitude
$U_{s,pulse}$	Dimensionless forced slip velocity
u	Local velocity in the x -direction (m s^{-1})
$u_{eff} = u_{b0}/\varepsilon$	Effective velocity (m s^{-1})

u_s	Slip velocity (m s^{-1})
$u_{s,A}$	Oscillation amplitude of slip velocity (m s^{-1})
v	Local velocity in the y-direction (m s^{-1})
w	Solute mass fraction
w_{ch}	Membrane channel width (m)
x	Distance in the bulk flow direction, parallel to membrane surface (m)
y	Distance from the bottom membrane surface, in direction normal to the surface (m)

Greek letters

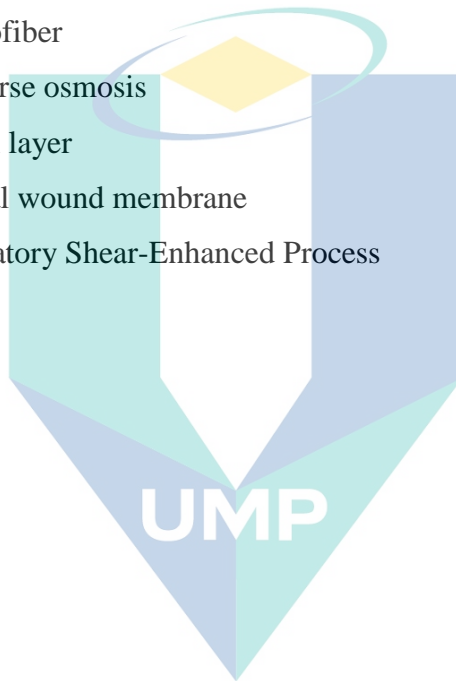
α	Specific flow attack angle
γ	Concentration polarisation index (modulus)
ε	Porosity
ε_e	Permittivity (F m^{-1})
ζ	Zeta potential (V)
μ	Dynamic viscosity ($\text{kg m}^{-1} \text{s}^{-1}$)
π	Osmotic pressure (Pa)
$\pi_0 = \phi w_{b0}$	Inlet osmotic pressure (Pa)
Π_{Lp}	Dimensionless membrane permeance
ρ	Fluid density (kg m^{-3})
σ	Reflection coefficient
τ	Wall shear stress (Pa)
ϕ	Osmotic pressure coefficient (Pa)
Φ	Local mass transfer enhancement factor
$\tilde{\Phi}$	Global mass transfer enhancement factor

Subscript

b_0	Value at inlet bulk conditions
EO	Value with forced slip velocity
max	Value for maximum variable
NS	Value without forced slip velocity (no-slip)
p	Value for the permeate
$pure$	Value for pure water
TA	Value for time-averaged variable
w	Value on the feed side membrane surface (wall)

LIST OF ABBREVIATIONS

CD	Charge density
CFD	Computational Fluid Dynamics
CP	Charge density
DL	Diffuse layer
EDL	Electric double layer
EOF	Electro-osmotic flow
HF	Hollow fiber
NF	Nanofiber
RO	Reverse osmosis
SL	Stern layer
SWM	Spiral wound membrane
VSEP	Vibratory Shear-Enhanced Process



اونيورسيتي مليسيا قهغ

UNIVERSITI MALAYSIA PAHANG

CHAPTER 1

INTRODUCTION

1.1 General Overview

Spiral wound membrane (SWM) modules are widely used in reverse osmosis (RO) desalting operations. However, a major problem for SWM is concentration polarization. Concentration polarization (CP) causes the decreases in permeate flux, thus increases the probability of fouling (Brian 1965; Matthiasson and Sivik 1980; Shaw, Deluca, and Gill 1972; Sherwood et al. 1965). CP can be reduced by increasing mass transfer coefficient and permeate flux.

Many ways have been studied to reduce the effect of concentration polarization. Some of the methods used are eddy promoters (spacers) and external electric field (Jagannadh and Muralidhara 1996). Liang et al. (Liang et al. 2014b; Liang et al. 2016; Liang, Fimbres Weihs, and Wiley 2014b, 2016) have shown that electro-osmotic flow can improve the permeate flux in membrane system. Among the variety of spacer configurations, zigzag configuration has been proved to be the most efficient in reducing CP (Schwinge, Wiley, and Fane 2004; Schwinge et al. 2000; Amokrane et al. 2015; Rodrigues et al. 2012).

External electric field technique such as electro-osmotic flow (EOF) is one of the techniques that can be used to enhance mixing within the membrane channel. The effect of steady EOF on permeate flux for high permeability membrane has been investigated (Liang et al. 2016), but the effect of transient EOF on mass transfer enhancement for high permeability membrane is yet to be fully investigated. It has been proven that the application at unsteady tend to be more effective at disturbing the boundary layer (Cohen-Tanugi et al. 2014), thus, the unsteady EOF can enhance mass transfer than steady EOF.

The usual parameters used to investigate the performance of a membrane module are mass transfer enhancement, relative change in permeate flux, maximum shear stress and Power number. Maximum shear stress is a proxy used to measure long term fouling reduction (Kraume and Drews 2010) while Power number is a proxy used to measure the energy losses (Fimbres-Weihs and Wiley 2010).

Computational Fluid Dynamics (CFD) has been widely used to gain insight into the flow inside membrane channel (Ahmad et al. 2005a; Schwinge, Wiley, and Fletcher 2002; Fimbres-Weihs, Wiley, and Fletcher 2006; Fimbres-Weihs and Wiley 2007; Vrouwenvelder et al. 2010; Parvareh et al. 2011; Yang et al. 2012; Li et al. 2012; Kostoglou and Karabelas 2012). This is because CFD is a powerful tool that can be used to generate the flow of a SWM module and visualize the mass transfer at the concentration boundary layer.

1.2 Problem Statement

Despite the numerous studies carried out to mitigate the effect of CP on the performance of a membrane system, the method of using a transient forced slip velocity to disrupt the boundary layer shows greater potential than any other methods.

This is because, it has been proven in the literature that creating flow disturbance in the membrane boundary layer is more effective for permeate flux enhancement than oscillating the bulk flow (Liang, Fimbres Weihs, and Wiley 2020). The recent advance in biotechnology and advanced material has resulted in a higher permeance, leading to significant permeate flux enhancement. However, a higher membrane permeance is also accompanied to a larger build-up of CP near the membrane surface. Thus, an innovation is needed to reduce the impact of CP for high-permeance membrane. One of the innovations is to use forced slip technique to renew boundary layer, thus improving mass transfer and reduce CP. The aim of this study is to understand whether membrane permeance affects unsteady mixing in the vicinity of the boundary layer of membrane channels, and to determine if such an approach has the potential to improve the permeate flux, even for high permeance or high flux membranes. It is crucial to note that this is not the only method that can be used to enhance mass transfer for a membrane system.

1.3 Research Objective

In this study, Computational Fluid Dynamic is used to investigate the potential of minimizing solute concentration at the membrane surface through the usage of electro-osmosis technique in the membrane systems. The specific objectives are:

- i. To determine the effect of different membrane permeance on resonant frequency of electro-osmotic flow slip velocity.
- ii. To determine the effect of membrane permeance on mass transfer enhancement, maximum shear stress and pumping energy generated by the slip velocity at the resonant frequency.

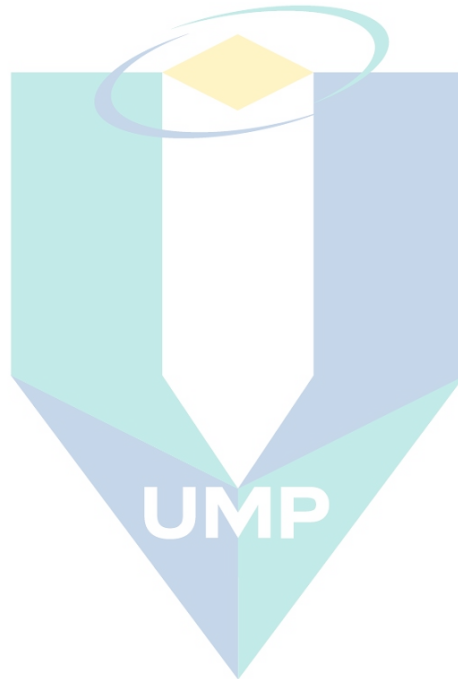
1.4 Scope of Study

In this thesis, the commercial Computational Fluid Dynamic (CFD) is employed to solve the fluid dynamics and mass transfer equations. CFD is also used to create a two-dimension flow geometry that illustrates the spacer-filled rectangular membrane which is used to represent the spiral wound membrane (SWM) module that is usually used in reverse osmosis (RO) operation. Furthermore, CFD is employed to solve the complex equations of Navier-Stokes and mass transfer equations. The detailed scopes of this study are as below:

- i. Frequency response test is used to obtain the first approximation peak frequency (resonant frequency). In this study, frequency response test is used to obtain the peak frequency range for each membrane permeance investigated (range of dimensionless membrane permeance investigated: $1.98 \times 10^{-5} - 3.53 \times 10^{-3}$).
- ii. Comparison of the effectiveness of membrane performance using relative change in permeate flux, maximum shear stress and Power number for different membrane permeance under the influence of forced-slip at the resonant frequency and Reynolds number of 408.

1.5 Novelty of this thesis

It has been shown that promoting unsteadiness in the presence of spacer leads to a larger boundary layer mixing and mass transfer enhancement. However, the study done by Liang et al. (Liang et al. 2014a) has only studied for a single membrane permeance, without taking into the interaction between spacer and unsteady flow (e.g. oscillating, vibration of forced-slip) for a larger membrane permeance. Thus, this thesis explores the effect of membrane permeance in the presence of forced-slip in spacer-filled channel by the means of CFD.



اونيورسيتي ملايسيا قهغ

UNIVERSITI MALAYSIA PAHANG

CHAPTER 2

LITERATURE REVIEW

2.1 Spiral Wound Membrane (SWM) Module

Spiral wound membranes (SWM) and hollow fiber (HF) modules are commonly used membrane modules in the world for separation purposes. Even though HF modules exhibit greater packing density than that of SWM modules, SWM modules are more preferable in many industries. This is because SWM modules have a better permeate rate, ease of operation and fouling control than that of HF modules (Schwinge et al. 2004). SWM modules are frequently used in many commercial water treatment and desalination processes for example, reverse osmosis (RO) and nanofiltration (NF). Reverse osmosis is an important process for producing fresh water according to Figure 2.1.

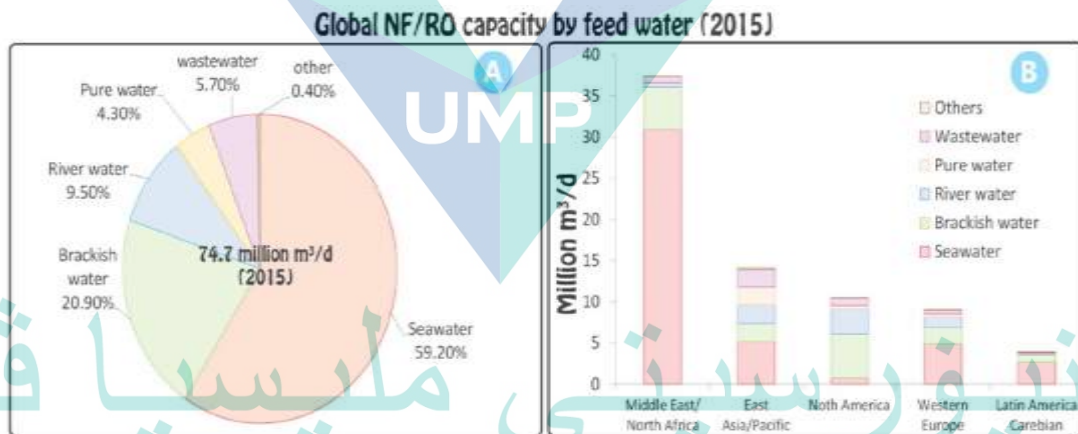


Figure 2.1 Types of feed water used (A) for NF/RO around the world and (B) in specific region

Source: DesalData (2015)

A generic SWM module is illustrated in Figure 2.2 (Johnson and Busch 2012). SWM module consists of a few major components, namely membrane sheets, spacer meshes and the permeate tube. A layer spacer mesh is wedged between two layers of membrane sheets and the membrane sheets are fastened together on several sides to form a membrane envelope. The open side of the membrane envelope is held on the permeate tube where permeate is accumulated. Several layers of membrane envelopes are then

tightly rolled up around the permeate tube and are secured by a pressurized module housing.

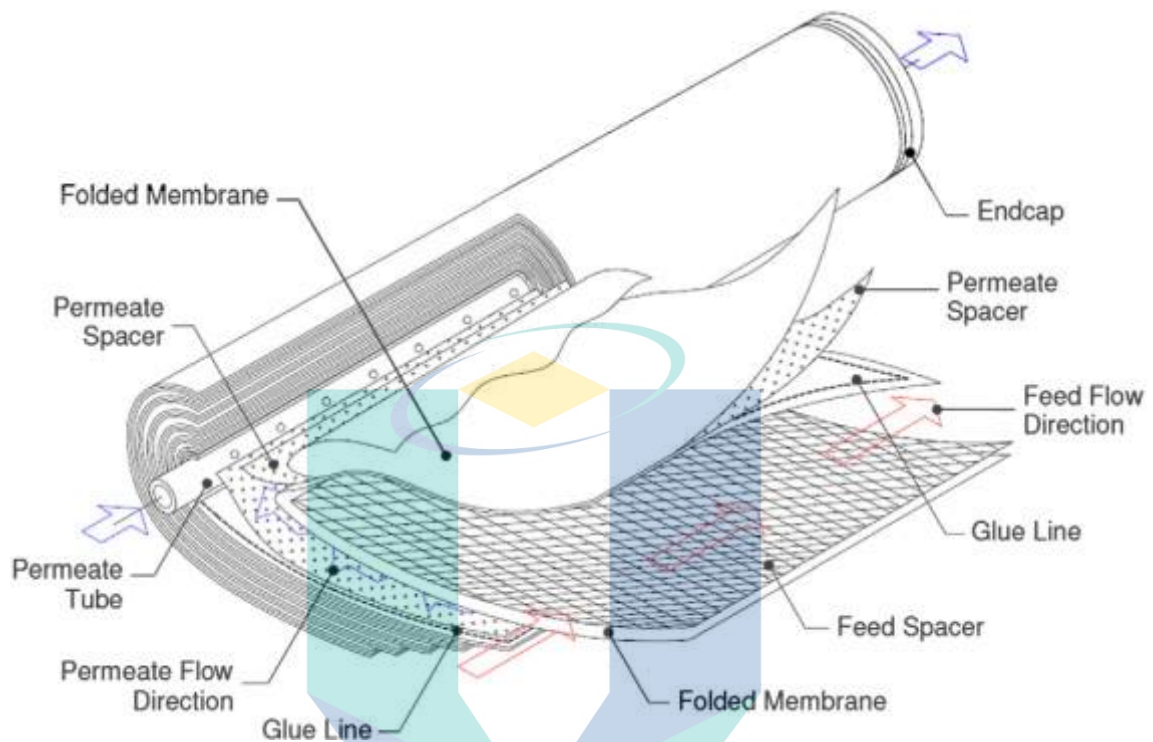


Figure 2.2 Spiral Wound Membrane (SWM)

Source: Johnson and Busch (2012)

CP and fouling are some of the main problems in SWM module. Concentration polarization occurs when there is accumulated solute in the vicinity of the membrane due to the presence of solute in the feed channel (Schwinge, Wiley, and Fane 2004). Both cause the flux to decrease throughout the membrane channel and thus, plummeting the performance of the membrane module. Typically, CP is mathematically expressed by w_w/w_b , where w_w refers to the solute concentration at the membrane surface whereas w_b refers to the solute concentration at the bulk flow.

Over the years, scientists and researchers have developed many methods to minimise the effects of CP and membrane fouling with the development in science and technology. Although study has found that the effects of concentration polarisation and fouling can be mitigated by enhancing the feed flow velocity, this method is not practical for SWM modules due to the very high pressure loss (Schwinge, Wiley, and Fane 2004). Therefore, other methods are needed to reduce the effect of concentration polarisation and membrane fouling without compromising the performance of the membrane modules.

Another method to enhance membrane performance is to introduce spacer into the membrane channel. The ideal spacer geometry for SWM modules has to have a high permeation with a relatively low pressure. This can be accomplished through the manipulation of the spacer filament diameters and mesh length between the filaments to achieve a higher flux and a lower pressure loss in SWMs.

The performance of SWM can be investigated by observing the fluid flow across a leaf in a flat channel test cell and its effect on the CP, permeate flux and pressure loss under a range of operating conditions. It must be noted that in actual industrial application, the membrane sheets of a spiral wound membrane module are coiled tightly around an inner perforated tube, thus, the membrane sheets are compressed and this will lead to the test cell results to be limited. For this reason, CFD can be used to investigate the local effect in SWM module.

2.2 Spacer geometry

It is known that spacer filaments are one of the essential elements in SWM modules to separate the membrane sheets apart and to create the flow channel (Haidari, Heijman, and van der Meer 2018; Gurreri et al. 2016; El Kadi, Janajreh, and Hashaikeh 2020). The spacer filaments are also known as eddy promoters as they induce crossflow velocity in membrane channel. The geometry of spacer in real life is depicted in Figure 2.3, which consist of two-layer of spacer (top and bottom) at a specified flow attack angle (α).

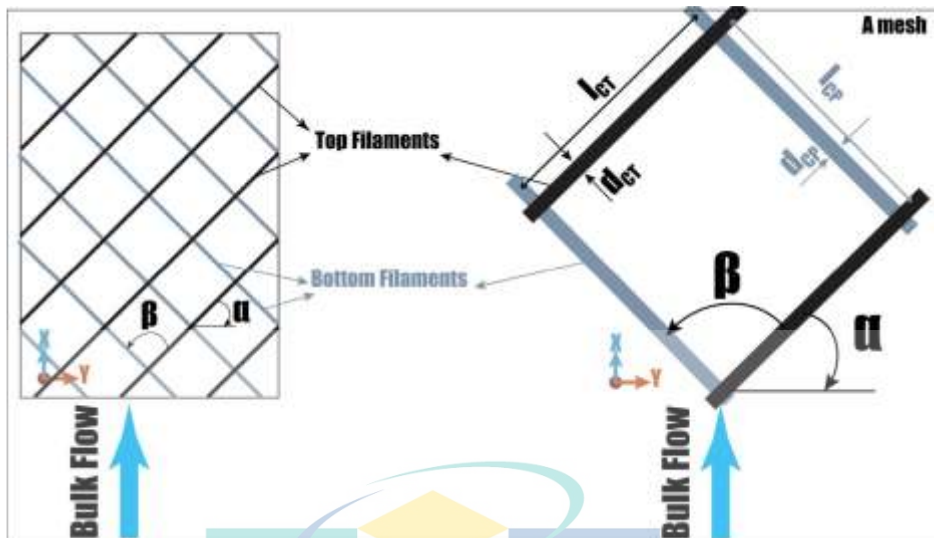


Figure 2.3 Spacer in SWM modules

Source: Haidari, Heijman, and van der Meer (2018)

The commonly used spacer filament geometries have the cross-section of a circle, square and triangle. These spacer filaments are then arranged in different configuration in the membrane channel and the performance of each configurations are evaluated. The most repeatedly studied spacer configuration are the submerged, zigzag, cavity type (Li and Tung 2008) as illustrated in Figure 2.4.

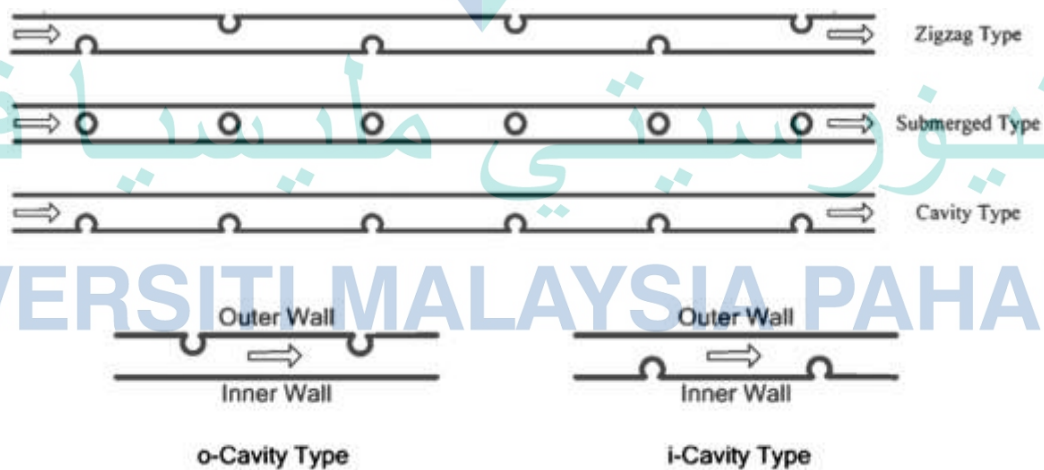


Figure 2.4 Spacer filament arrangement in a two-dimensional channel

Source: Li and Tung (2008)

Geraldes et al. (Geraldes, Semião, and de Pinho 2002; Geraldes, Semião, and Norberta Pinho 2003; Geraldes, Semiao, and Norberta de Pinho 2004) have carried out experimental studies on the effects of concentration polarisation. The mass transfer was enhanced in the region next to spacer. These observations were further confirmed by Ahmad et al. (Ahmad and Lau 2006; Ahmad et al. 2005b). Ahmad et al. (Ahmad and Lau 2006; Ahmad et al. 2005b) have conducted the study on the effect of three two-dimensional spacer configurations, namely a circular, a square and a triangle geometry filaments (see Figure 2.5) only touching one wall of the membrane channel, on concentration polarisation and permeation under steady (Ahmad et al. 2005b) and unsteady (Ahmad and Lau 2006) state hydrodynamics. These show that spacer filaments have the potential to enhance the mass transport and reduce concentration polarisation in channel. For SWM modules operating under the prevailing Reynolds number (below 400), the cylindrical filaments has smaller concentration factor when compared with other filament geometries (Ahmad and Lau 2006).

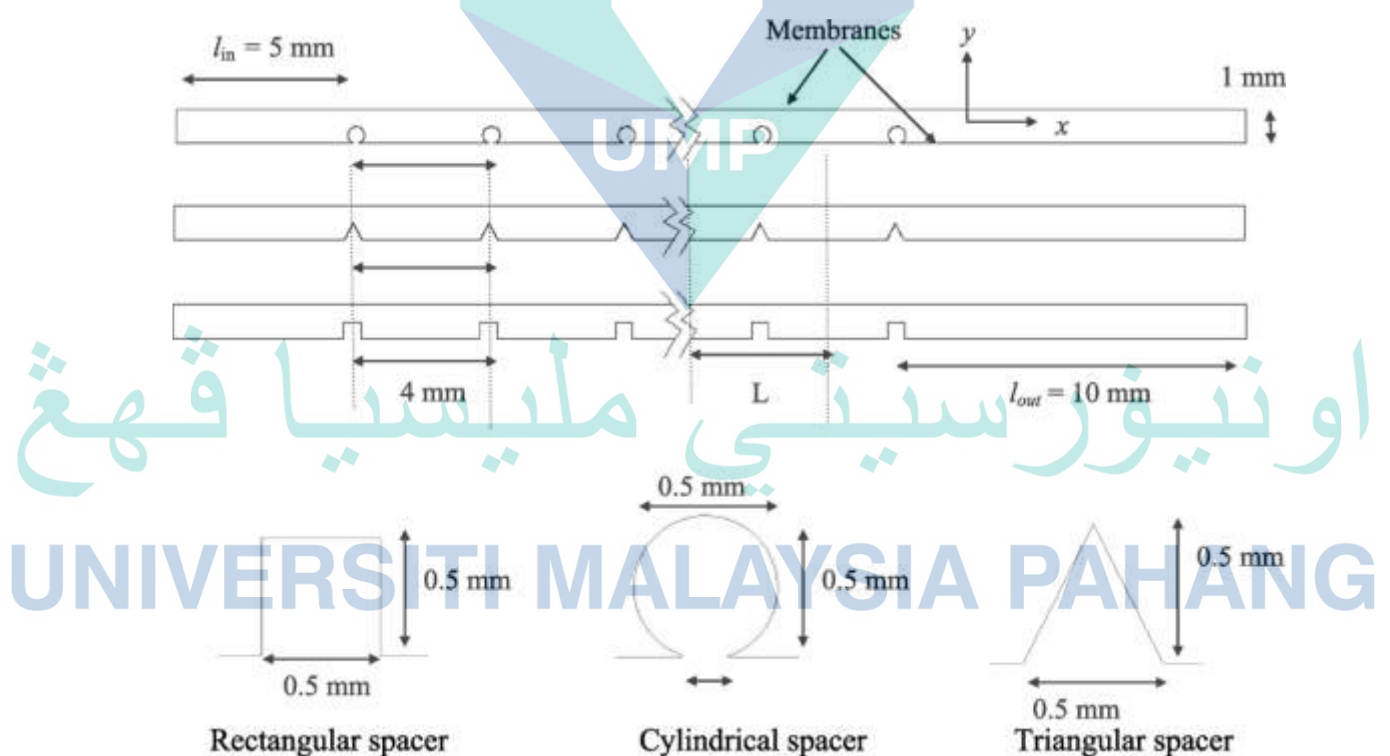


Figure 2.5 Rectangular, Cylindrical and triangular spacer

Source: Ahmad and Lau (2006); Ahmad et al. (2005b)

Ma et al. (Ma and Song 2006; Ma et al. 2004) have conducted the analysis of the effect of two filament configurations, namely the submerged type and the zigzag type, and of the voidage between square filaments. From their analysis, the zigzag configuration has the tendency to minimise the concentration polarisation. Furthermore, a two-dimensional steady-state model was obtained by Wardeh and Morvan (Wardeh and Morvan 2008), based on the rectangular channel used in Fletcher and Wiley's study (Fletcher and Wiley 2004). The model was used to model the permeation and concentration polarisation (Wardeh and Morvan 2008). The effect of cylindrical submerged and zigzag spacer configuration on mass transfer was investigated by these authors using an expanded version of the membrane model. Their result shows that the zigzag configuration is more effective in reducing salt concentration at the membrane wall compared to the other configuration. These studies show that the zigzag spacer configurations are ideal to be used in SWM modules for desalination purposes.

One of the important functions of spacer is to promote flow unsteadiness (see Figure 2.6). For example, Fimbres-Weihs et al. (Fimbres-Weihs, Wiley, and Fletcher 2006) found that at a higher Reynolds number, the location of a greater mass transfer does not depend only on large shear-rate but also to the direction where flow with low concentration towards the membrane surface. They concluded there are two main mechanisms that lead to higher mass transfer, namely: 1) high shear rate; and 2) flow of low concentration towards membrane concentration polarisation layer.

اونيور سیتی ملیسیا قهغ

UNIVERSITI MALAYSIA PAHANG

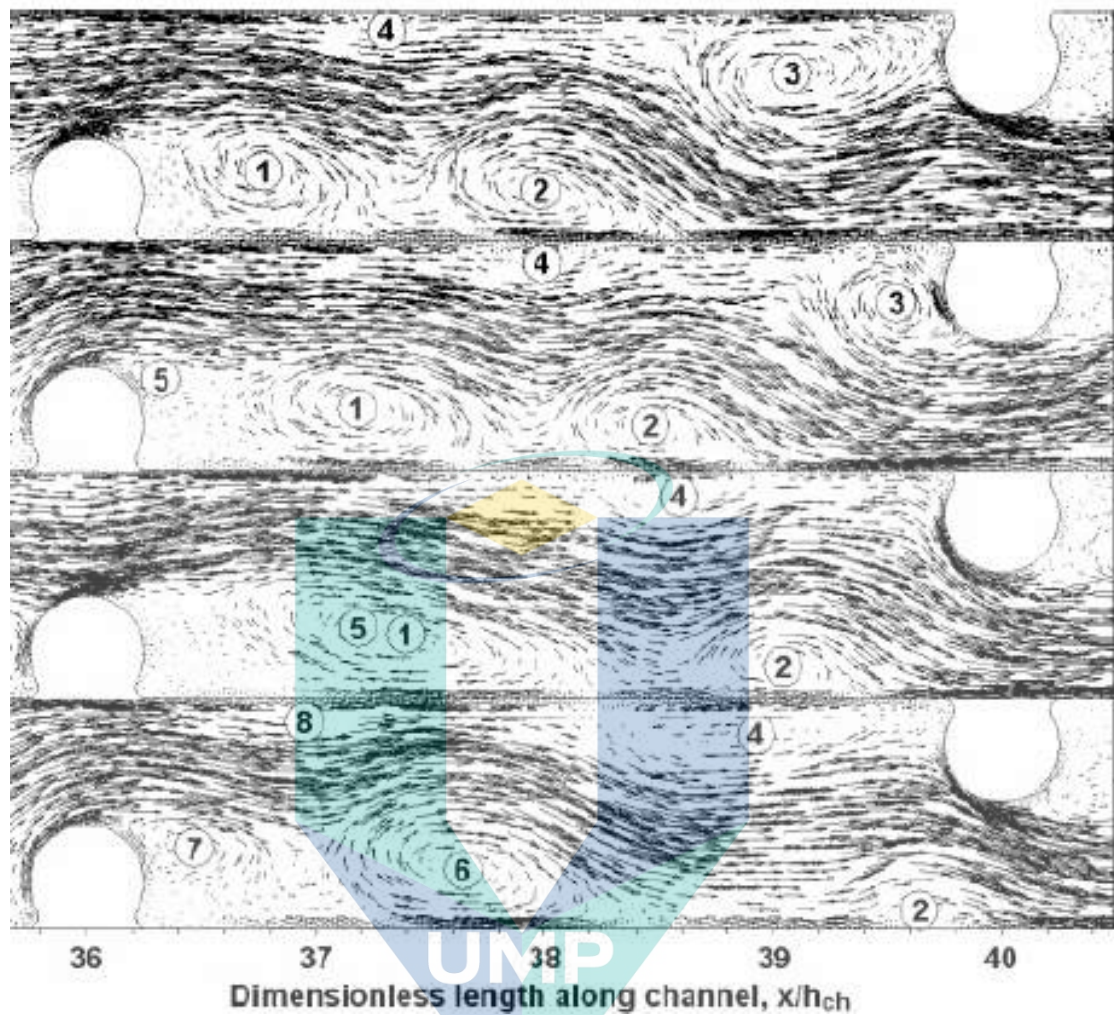


Figure 2.6 Velocity vector plot at Re 841. Number 1-8 represents the shed vortices

Source: Fimbres-Weihs, Wiley, and Fletcher (2006)

2.3 Computational Fluid Dynamics (CFD) study of spacer-filled channel

2.3.1 Computational Fluid Dynamics (CFD) basics

Computational Fluid Dynamics (CFD) is the numerical technique that can solve the continuity, momentum, energy and species transport (Banik, Bandyopadhyay, and Biswal 2019; Keir and Jegatheesan 2013; La Cerva et al. 2019; Pawlowski et al. 2016; Suresh, Selvam, and Karunanithi 2019). From the works by Wiley and Fletcher (Wiley and Fletcher 2003; Fletcher and Wiley 2004), they have proven that both gravity and density variation do not have significant effect on the solution obtained. Therefore, the assumption of negligible gravity and constant fluid properties are in use. Moreover, to further simplify the system, the flow is assumed to be two-dimensional and the fluid is

assumed to be Newtonian (Fimbres-Weihs, Wiley, and Fletcher 2006; Fimbres-Weihs and Wiley 2010). Thus, the Navier Stokes and momentum transport equation are expressed as equations 2.1 and 2.2:

$$\rho \frac{\partial \vec{v}}{\partial t} + \rho(\vec{v} \cdot \nabla)\vec{v} = \mu \nabla^2 \vec{v} - \nabla p \quad 2.1$$

$$F \rho \frac{\partial w}{\partial t} + \rho \nabla \cdot (w\vec{v}) = D \nabla^2 w \quad 2.2$$

where ρ , v , w , D , t refer to density, velocity, solute mass fraction, diffusivity and time, respectively.

There are some forms of the transport equation available subject to choice of transported variable and reference velocity, such as mass fraction, mass concentration, molar fraction, and molar concentration. Details of these forms for species transport equation can be found elsewhere (Fimbres-Weihs and Wiley 2010).

2.3.2 Mesh Independence study

Mesh independence study needs to be performed to ensure that the solution used in the study is independent of the mesh used. This is important to reduce numerical error caused by mesh.

Verification for Computational Fluid Dynamics (CFD) simulation is carried out to make sure that the computational code is accurately solving the transport equations which are a system of partial differential equations. Several common sources are (Oberkampf and Trucano 2002):

- i. inadequate spatial discretization convergence
- ii. inadequate temporal discretization convergence
- iii. inadequate convergence
- iv. round-off, and
- v. programming errors

Grid Convergence Index (GCI) is used to predict the error with the grid used based on the Richardson's extrapolation (Roache and Knupp 1993) and developed by Roache (Roache 1997). The GCI for fine (GCI_{fine}) and coarse grids (GCI_{coarse}) can be expressed by (Roache and Knupp 1993):

$$GCI_{fine} = \frac{3|e|}{R^\eta - 1} \quad 2.3$$

$$GCI_{coarse} = \frac{3|e|R^\eta}{R^\eta - 1} \quad 2.4$$

where

$$R = \frac{N_{fine}}{N_{course}} \quad 2.5$$

$$e = F_{course} \frac{F_{fine}}{F_{course}} \quad 2.6$$

The dimensional number (η) used in equation 2.3 and 2.4 is either 2 for two dimensional and 3 for three dimensional. Verification can be performed by consecutively enhancing spatial and/or temporal resolution so that the GCI for the fine mesh reduces to a low error (5-10%). Validation can also be carried out by performing comparison numerical model solution with the experimental results, also known as the "correct answer". However, such solutions are not often obtainable. The typical diagram for verification and validation is shown in Figure 2.7.

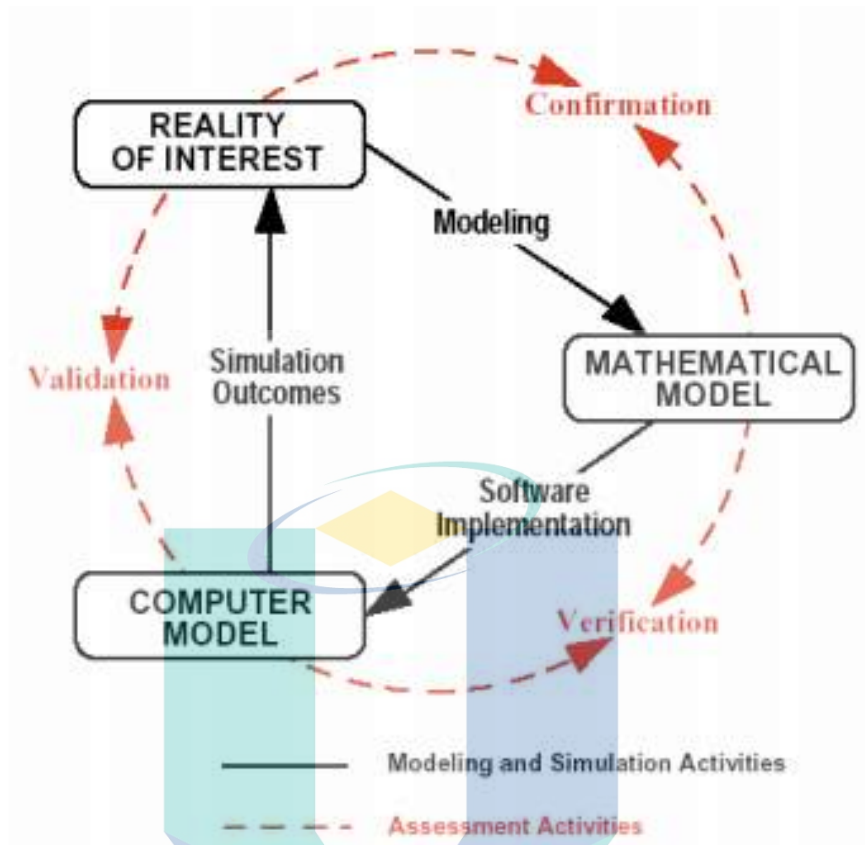


Figure 2.7 Verification and validation

Source: Schlesinger (1979)

2.4 External techniques for creating flow unsteadiness

2.4.1 Vibration method

One of the methods to create unsteadiness is through vibration of a membrane surface. This method has the potential to produce unsteady-shear on the membrane wall to reduce the effect of CP and fouling, especially when this method is employed at the amplitude and frequency is more than a critical value (Genkin et al. 2006). Vibratory Shear-Enhanced Process (VSEP) and submerged vibration systems (for both hollow fibre and flat sheet membranes) are two of the many systems that used the vibration method and are popular among researchers.

The VSEP system was developed in the early 1990s by Culkin and Armando (Culkin and Armando 1992), and was later commercialized for industrial application by New Logic Research Inc.. Studies of the effectiveness of VSEP system have been carried

out in microfiltration (Zouboulis and Petala 2008), ultrafiltration (Zouboulis and Petala 2008), nanofiltration (Zouboulis and Petala 2008; Ahmed et al. 2010) and reverse osmosis (Shi and Benjamin 2011) membranes. A VSEP unit is generally made up a filter pack and a motor (Culkin and Armando 1992). The filter pack is fixed on a shaft and is oscillated on its axis by a motor (Culkin and Armando 1992). Spacers in the filter pack acts a separator for the membrane leaves to provide flow channels (Culkin and Armando 1992). The shear generated by vibration motion of the filter pack in the direction tangent to the membrane surface has the potential to reduce CP and fouling. This shows that the shear rate induced on the membrane surface is the key parameter to reduce CP and fouling in vibration system (Jaffrin 2008). A higher vibration amplitude is more beneficial in an application which is more prone to membrane fouling (Low, Jin, and Tan 2004).

The shear rate induced on the membrane wall is one of the key factor that mitigate fouling (Jaffrin 2008). Studies (Akoum et al. 2002; Postlethwaite et al. 2004; Jaffrin et al. 2004; Akoum, Jaffrin, and Ding 2005; Petala and Zouboulis 2006) have shown that the permeate flux enhances with maximum shear rate and the maximum achievable shear rate through VSEP is approximately 10^5 s^{-1} . Those studies (Akoum et al. 2002; Postlethwaite et al. 2004; Jaffrin et al. 2004; Akoum, Jaffrin, and Ding 2005; Petala and Zouboulis 2006) also show that when the flow regimen transited from laminar to turbulent flow, the enhanced secondary flow generated has the potential to enhance solute back-transport from the surface.

There are generally two types of submerged vibration systems, which are the submerged flat sheet membranes (Gomaa and Rao 2011; Gomaa 2012; Gomaa, Rao, and Taweel 2011) and hollow fibre membranes (vibrated both axially (Li et al. 2013; Beier et al. 2006; Beier and Jonsson 2006; Prip Beier and Jonsson 2009; Low, Juan, and Siong 2005) and transversely (Kola et al. 2012; Kola et al. 2014; Li, Law, and Fane 2014; Low, Juan, and Siong 2005)). The transversely vibrating hollow-fibre systems on the other hand have additional induced secondary flows, thus, showing a significant improvement in fouling mitigation (Kola et al. 2014).

There are a few key points on the permeate flux enhancement via vibration method. Firstly, the mechanisms in vibration systems that lead to CP and fouling mitigation are the back-diffusion triggered by the pulsation and the induced unsteady shear on the wall (Genkin et al. 2006; Akoum et al. 2002). Secondly, the transverse vibration systems are

more effective in enhancing the flux than the axial vibration systems when applied at the exact frequency and amplitude due to the secondary flow in the transverse vibration systems (Kola et al. 2012; Kola et al. 2014; Li, Law, and Fane 2014). Next, the achievable flux enhancement via vibration method depends on the transmembrane pressure (TMP) in the filtration process (Akoum, Jaffrin, and Ding 2005), as CP reduction is more efficient for systems with higher TMP. Finally, the turbulent promoters in the membrane channels can further enhance the permeate flux (Gomaa 2012; Gomaa, Rao, and Taweel 2011).

However, with the current technology available around the world, one of the drawbacks in the VSEP method is that this method is limited to small scale processes. This drawback can be overcome by using multiple modules together. The other drawback is the module design which has a lower packing density compared to the SWM and hollow fibre membranes. Finally, VSEP is not suitable to be applied in high pressure containment.

Su et al. conducted vibration study experimentally (See Figure 2.8) and varied vibration frequency to study system performance under varying operating condition (Su et al. 2019). They found that a high-frequency of vibration has potential to reduce sodium chloride accumulation and higher permeation when colloidal fouling presents. For example, as shown in Figure 2.9, there is less porous cake layer growth when vibration is conducted at 60 Hz compared to case without vibration in their CFD simulation. This is however, the enhancement is lesser for system at high flow rate (Reynolds number) because the shear caused near the membrane wall is already very high at high Reynolds number.

اوتنور سيني مليسيا هغ

UNIVERSITI MALAYSIA PAHANG

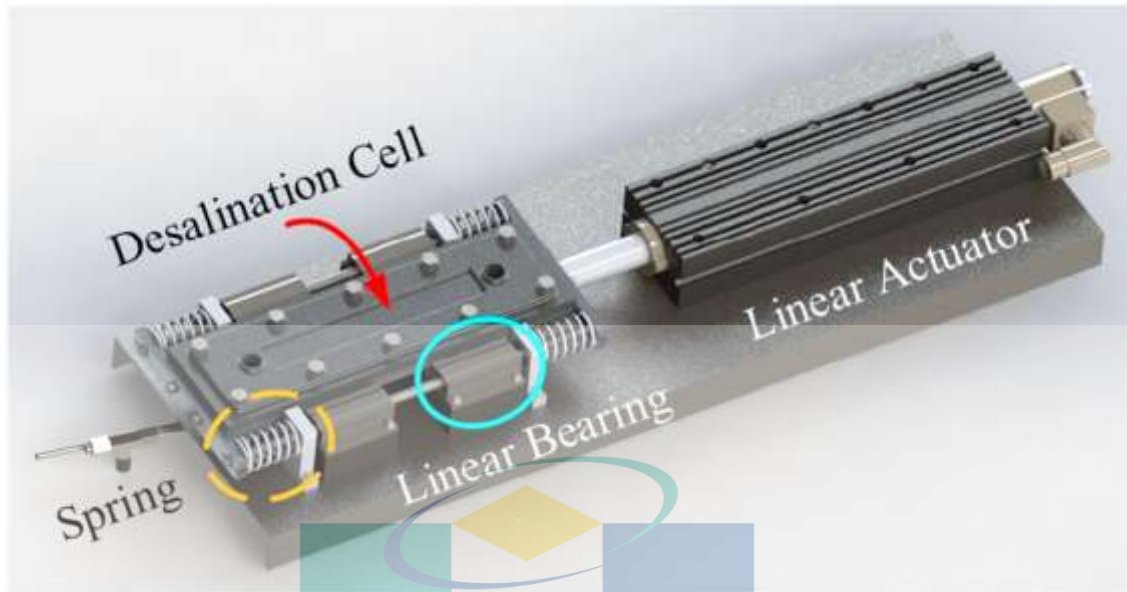


Figure 2.8 Vibration device within desalination cell

Source: Su et al. (2019)

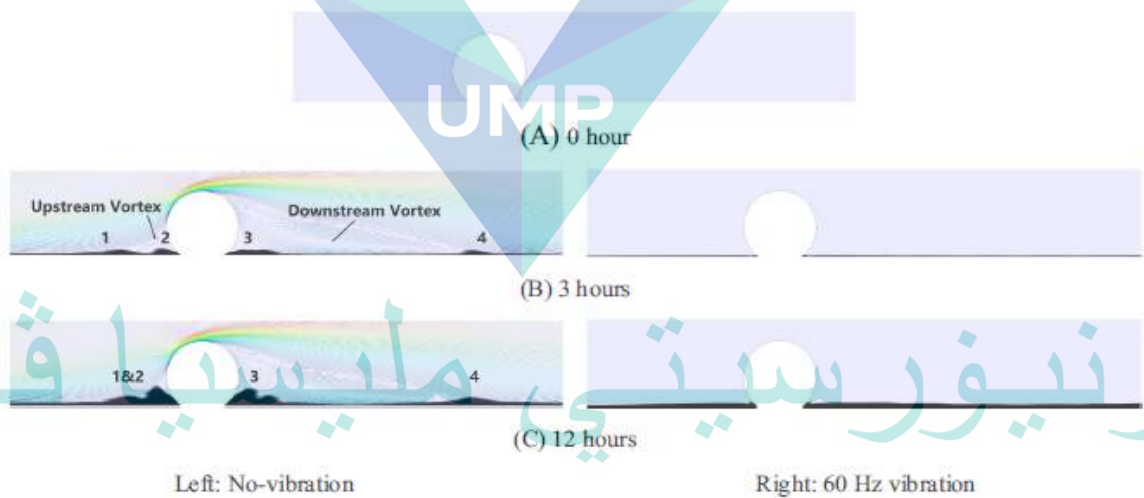


Figure 2.9 Porous cake layer growth for case without vibration and with vibration

Source: Su et al. (2019)

The vibration occurring at the membrane surface has impact on the CP boundary layer and is effective in increasing the enhancement factors. However, vibration method does not perform well in RO process. Thus, it is more practical to implement this method in hollow fibre membranes which have been proven to be more effective in flux enhancement due to the increased secondary flow effects.

2.4.2 Pulsation method

Another approach that has the potential to reduce the effect of concentration polarisation thru unsteady state shear method is the pulsation method. Pulsation method is one of the cost effective filtration processes that can be applied in reverse osmosis, ultrafiltration and microfiltration (Al-haj Ali et al. 2013, 2011; Thomas and Jain 2007; Gupta, Blanpain, and Jaffrin 1992; Huang and Chen 2013; Saremirad, Gomaa, and Zhu 2012). The mechanism of oscillating flow can be described in Figure 2.10, where oscillating flow causes a velocity profile with two equal maxima near the membrane surface than in the bulk flow. However, the effect of the oscillated back flushing is not present in the RO processes as it is only applicable in microporous membranes.

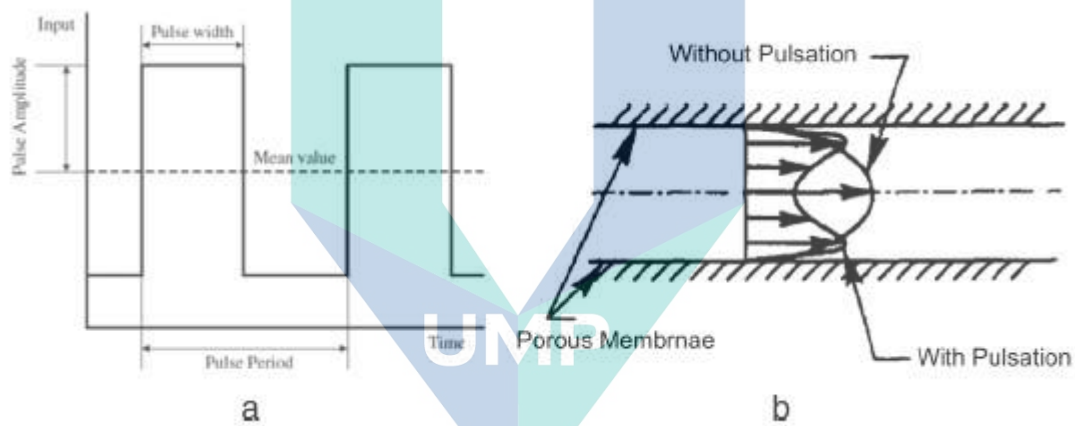


Figure 2.10 Velocity profile in the presence and absence of oscillating flow

Source: Winzeler and Belfort (1993)

It should be noted that the unsteady shear reduces the concentration boundary layer and increases the back-transport of the solutes and particulates. The enhanced shear rate at the membrane wall resulting in the transport of solute to the bulk flow will minimize the effect of concentration polarisation and membrane fouling (Finnigan and Howell 1990). This effect is also known as the Richardson effect (Finnigan and Howell 1990). In some cases, negative transmembrane pressure is generated and this will result in the reverse flux which acts as the back washing, the effect that forces the deposits on wall.

Ilias and Govind (Ilias and Govind 1990) have indicated the importance of choosing the suitable waveforms and frequency applied the membrane module used. There are a few parameters that must be considered that will affect the generated pressure waveform which are the maximum and minimum pressure, the duration of pressures and the frequency (Li, Bertram, and Wiley 1998). This is because the generated waveforms will affect the concentration-polarisation-boundary-layer and cake removal (Li, Bertram, and Wiley 1998). However, pressure pulsation to create pulsations has no significant effect on the streamline near the membrane boundary layer where concentration polarisation occurs (Zamani et al. 2015). On the other hand, pulsatile flow does affect the velocity profile near the wall, thus, affecting the shear on the membrane surface via the Richardson effect (Zamani et al. 2015).

For the case of RO processes, there are several numerical studies in empty channels (Liang, Fimbres Weihs, and Wiley 2016; Liang et al. 2014b) and experimental studies in spacer-filled channel (Liang, Fimbres Weihs, and Wiley 2016) showing that the pulsatile flow can increase mass transfer. There is a difference in operating condition between the laminar and turbulent regimes. For the laminar flow, a noticeable improvement in performance is observed at the frequencies above 5 cycles/min (Kennedy, Merson, and McCoy 1974). For the turbulent flow, no enhancement is observed at the frequencies below 10 cycles/min (Kennedy, Merson, and McCoy 1974). When the pulsatile flow under laminar flow regime is applied at the frequency of 1 Hz, the permeate flux can be enhanced by more than 68 % (Ilias and Govind 1990). It is shown that pulsation method under the cyclic operation also led to a flux enhancement of about 6.5 % with a low pulsation frequency of a period of 5 min (Al-Bastak and Abbas 1998).

On the other hand, a seawater reverse osmosis membrane system operating with pulsation increased the permeate flux by about 10 % and minimised the salt passage slightly with an associated of an increased the energy consumption (Abbas and Al-Bastaki 2000). When frequency of the pulsation is increased (maximum of 1 Hz), the permeate flux can increased up to 60 – 80 % (Abbas and Al-Bastaki 2000). Their permeate flow rate increased by 42 % and the salt concentration in the permeate reduced by 20 % (Al-haj Ali et al. 2013).

From Fimbres-Weihs and Álvarez-Sánchez (Fimbres-Weihs and Álvarez-Sánchez 2017) recent work, they have discovered that the pulsation method can improve RO membrane productivity without greatly increasing the energy costs when applied at the resonant frequency. In their case study, they discovered that to enhance the flux by 24 % for the module applied at the Reynolds number around 350 – 400, the pulsation method requires the pulsation frequency between 14 -16 Hz with an associated increased pumping cost around 10 – 15 %; without external perturbation, the Reynolds number has to increase about 150 to achieve the equivalent enhanced flux with an associated increased pumping cost over 130 %. This indicates that the pulsation method applied at the specific frequency has a lesser impact on the pumping cost compared to the method of increasing the module Reynolds number.

2.4.3 Electro-osmotic flow (EOF) forced slip

Electrokinetic phenomena occur when the motion of the liquid is indirectly influenced by an external electric field generated near a solid-fluid interface (such as a membrane surface). One of the main problems affecting the numerical modelling of EOF flow is the large computational load due to the complex relationship between the flow and electric field (Liang, Fimbres Weihs, and Wiley 2014b). The basic concept of electro-osmosis can be described as below:

EOF is defined as the movement of liquid responding to an electric field. The phenomenon where ions attract and repulse each other near a charged surface is due to the presence of similarly charged ions and oppositely charged ions. As a result, an electric double layer (EDL) is created. The amount of counter-ions present is greater than that of co-ions, so that the surface charge is neutralized (Probstein 1989). Stern layer (SL), is also known as the inner most part of EDL which is adjacent to the surface; while diffuse layer (DL), is the outer layer which is away from the surface. The schematic diagram of electric double layer is shown in Figure 2.11.

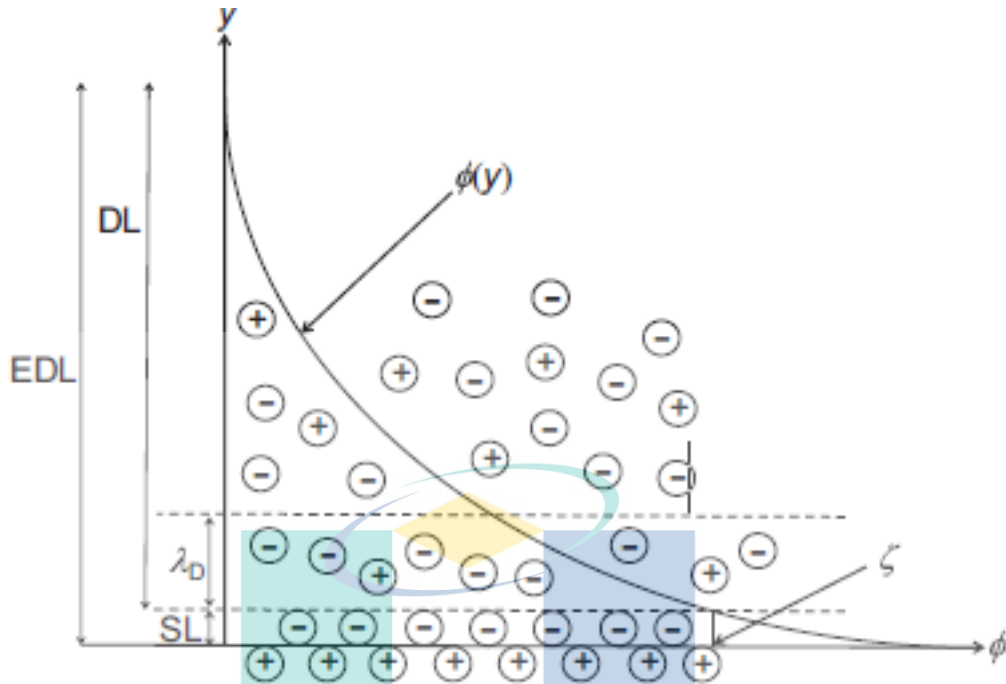


Figure 2.11 Electric double layer structure

Source: Liang, Fimbres Weihs, and Wiley (2014b)

Poisson's equation for electrostatics is expressed in the following approach (Hunter 1981):

$$\nabla^2 \phi = \frac{-\rho_e}{\epsilon} \quad 2.7$$

where ϕ , ρ_e , and ϵ refer to the potential due to the double layer, electric charge density and the permittivity of the fluid, respectively.

The electric charge density (ρ_e) can be shown in the form of a Boltzmann distribution (Probstein 1989):

$$\rho_e = -2zen_o \sinh\left(\frac{ze\phi}{k_B T}\right) \quad 2.8$$

where n_o is the ion concentration, z is the ionic valence, e is the electron charge, k_B is the Boltzmann constant and T is the temperature.

The approximation of $\sinh(a) \approx a$ for $\phi \ll \frac{k_B T}{\varepsilon}$ can be used to linearized the system of equation 2.7 and 2.8. Assumption of the electric potential to be constant along the x direction is taken into account, thus equation 2.7 and 2.8 can be reduced the following expression:

$$\phi = \zeta \exp\left(\frac{-y}{\lambda_D}\right) \quad 2.9$$

The charge density (CD) solution in equation 2.9 employed in this study is the analytical solution of the 1D case of equation 2.7 and 2.8. The Debye length can be computed as (Russel, Saville, and Schowalter 1992):

$$\lambda_D = \sqrt{\frac{\varepsilon k_B T}{2e^2 n_o}} \quad 2.10$$

Electro-osmosis effects can be incorporated to the momentum transport equation as:

$$\rho \left(\frac{\partial \vec{v}}{\partial t} + \vec{v} \cdot \nabla \vec{v} \right) = -\nabla P + \mu \nabla^2 \vec{v} + \rho_e \vec{E} + \rho g \quad 2.11$$

where P is the pressure, \vec{v} us the velocity, μ is the viscosity, \vec{E} is the electric field, ρ is the density and g is the gravitational acceleration.

The electric field (\vec{E}) can be stated as in equation 2.12:

$$\vec{E} = -\nabla(\phi + \psi) \quad 2.12$$

where ψ is the potential due to the external electric field (Rawool and Mitra 2006; Patankar and Hu 1998).

The following equation, equation 2.11, can be used to approximate the slip velocity boundary condition (Probstein 1989).

$$u_s = \frac{\varepsilon \zeta E_x}{\mu} \quad 2.13$$

where ε , ζ , μ and E_x are porosity, seta potential, viscosity and electric field component in the x-direction.

Equation 2.13 can be denoted as a “linear electro-osmosis” (Hu and Li 2007). Based on the finding by Liang et al. in 2013 (Liang, Fimbres Weihs, and Wiley 2014b), the HS approximation agrees with the CD solution for both cases conducted in the 2013 study. Therefore, the HS approximation is a reliable approach to calculate the electro-osmosis flow at the membrane surface. Later, Liang found that electro-osmotic slip velocity has potential to increase permeate flux by 21 % when a suitable peak frequency is chosen in spacer-filled channel from frequency response analysis. It is important to note that the effect of slip velocity on flow and mass transfer enhancement has been validated in an empty channel (Liang et al. 2014b).

A summary of the effect of different perturbation techniques are included in Table 2.1.

Table 2.1 Summary of the effect of different perturbation technique

Technique	Author	Findings
Slip velocity	Liang, Fimbres Weihs, and Wiley (2014b)	Found that electro-osmotic slip velocity to increase permeate flux by 21 % when a suitable peak frequency is chosen in spacer-filled channel.
Pulsatile flow	Finnigan and Howell (1990).	Showed that the enhanced shear rate at the membrane wall to reduce the fouling.
	Ilias and Govind (1990)	Found that the permeate flux can be enhanced by more than 68 % when frequency of 1Hz is applied
	Li, Bertram, and Wiley (1998)	Found that the generated waveforms will affect the concentration-polarisation-boundary-layer.
	Kennedy, Merson, and McCoy (1974)	Found a noticeable improvement in performance at the frequencies above 5 cycles/min
	Al-Bastak and Abbas (1998).	Found that flux is improved by 6.5% under the cyclic operation with a period of 5 min.
Vibration	Abbas and Al-Bastaki (2000).	Found that the flux increased by 42 % and the permeate salt concentration reduced by 20 %.
	Culkin and Armando (1992)	Developed the Vibratory Shear-Enhanced Process in the early 1990s.
	Jaffrin (2008).	Found that shear rate induced on the membrane surface is the key parameter to reduce CP and fouling in vibration system.
	Low, Jin, and Tan (2004)	Found that a higher vibration amplitude is more beneficial for application prone to membrane fouling.
	Kola et al. (2012); Kola et al. (2014); Li, Law, and Fane (2014)	Found that transverse vibration systems are more effective in enhancing the flux than the axial vibration systems.
Su et al. (2019)	Found that a high-frequency of vibration has potential to reduce sodium chloride accumulation.	

2.5 Gap analysis

Recently, with advancements in the fields of nanotechnology and biotechnology, scientists and researchers have suggested that ultra-permeable membranes (UPMs) will be the next generation reverse osmosis (RO) membranes for desalination. However, with higher L_p , concentration polarisation also increases. To address this problem, innovation is needed to reduce CP for membranes with higher L_p . Such innovation can potentially be achieved by the application of unsteady shear strategies. Electro-osmotic flow (EOF) is one of the hydrodynamic methods that can be used to generate a forced slip velocity. Under EOF conditions, an applied external electrical field induces an electro-osmotic slip velocity near a charged surface, where it can perturb the flow, promote boundary layer renewal and, therefore, increase mixing and mass transfer. This study aims to use CFD to understand whether membrane permeance or high flux affects unsteady mixing in the vicinity of the boundary layer of membrane channels, and to determine if such an approach has the potential to improve the permeate flux, even for high permeance membranes. Although this study uses an unsteady forced slip velocity to disrupt the boundary layer, it shall be noted that this is not the only method that can be used to enhance mass transfer for a membrane system. Other hydrodynamic-based approaches, such as pulsation and vibration methods, can also be used to induce vortex shedding, change the flow in the boundary layer and, thus, improve mass transfer and reduce concentration polarisation.

اونيورسيتي ملايسيا قهغ

UNIVERSITI MALAYSIA PAHANG

CHAPTER 3

METHODOLOGY

3.1 Model description

The CFD (ANSYS CFX 16.2) is used to simulated a two-dimensional, constant property transient Newtonian fluid flow inside a narrow spacer-filled membrane channel, following the method and assumptions of the studies carried out by Liang et al. (Liang, Fimbres Weihs, and Wiley 2014a, 2016). The software package solves the coupled continuity, momentum and mass transfer equations for a given set of initial and boundary conditions. For constant property Newtonian fluid flow, these governing equations are as follows:

$$\nabla \cdot \vec{v} = 0 \quad 3.1$$

$$\rho \frac{\partial \vec{v}}{\partial t} + \rho(\vec{v} \cdot \nabla)\vec{v} = \mu \nabla^2 \vec{v} - \nabla p \quad 3.2$$

$$\rho \frac{\partial w}{\partial t} + \rho \nabla \cdot (w\vec{v}) = D \nabla^2 w \quad 3.3$$

where ρ , v , w and t refer to density, velocity, solute mass fraction and time, respectively.

Figure 3.1 and Figure 3.2 illustrate the channel and electrode geometry used in this study, which has the same geometry as in (Haidari, Heijman, and van der Meer 2016). Further details on the model parameters are presented in Table 3.1 based on typical membrane and operating conditions (Liang, Fimbres Weihs, and Wiley 2016). The region around the unit cell containing spacer 7 and 8 is used for detailed analysis of the local and global variables. The size of the time step used corresponds to the time step when the RMS courant number is below 1. With respect to advection scheme, a high-resolution scheme is used in this simulation study.

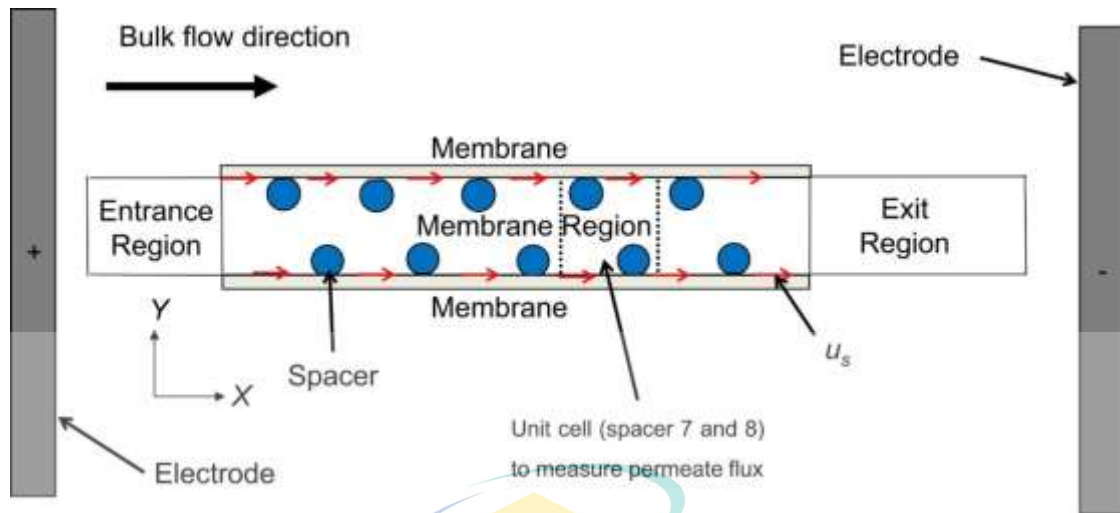


Figure 3.1 Schematic of fluid domain (not to scale) indicating boundary locations and channel regions. Red arrows on the membrane surface indicate the location of slip velocity

Source: Liang et al. (2016)

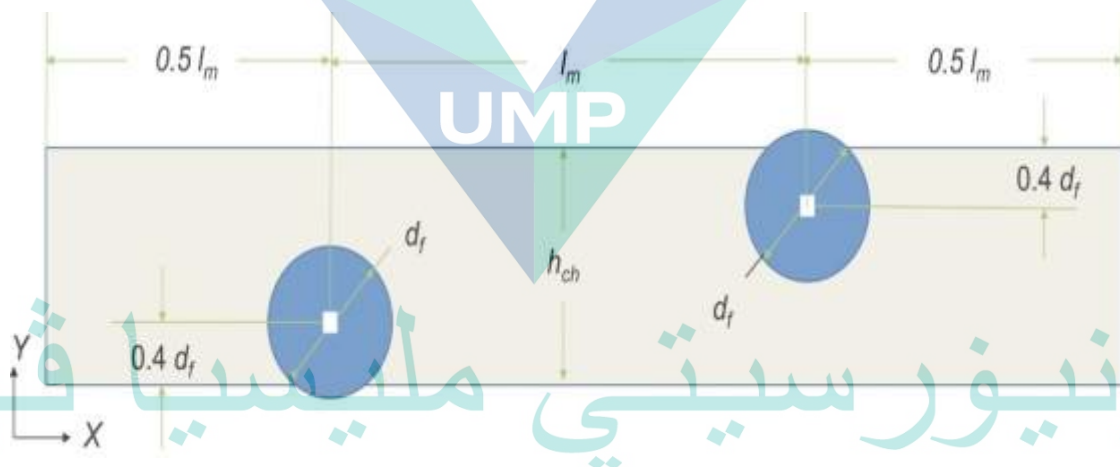


Figure 3.2 Geometry of the spacer unit cell

Source: Liang et al. (2016)

Table 3.1 Parameters used for slip velocity case study

Parameter	Value
Feed Solute Mass Fraction (w_{b0})	0.01, 0.025, 0.04
Dimensionless Inlet Transmembrane Pressure ($P_0 = \frac{\Delta p_{tm}}{\pi_0}$)	1.46, 1.86, 3.65
Dimensionless Forced Slip Velocity Amplitude ($U_{s,A} = \frac{u_{s,A}}{u_{eff}}$)	5.55×10^{-3}
Intrinsic Rejection (R)	0.996
Dimensionless Membrane Permeance ($\Pi_{Lp} = \frac{L_p \pi_0}{u_{eff}}$)	$1.98 \times 10^{-5} - 3.53 \times 10^{-3}$
Reflection Coefficient (σ)	1
Hydraulic Reynolds number ($Re_h = \frac{\rho u_{eff} d_h}{\mu}$)	408
Slip Reynolds number ($Re_s = \frac{\rho u_{s,A} d_h}{\mu}$)	2

In this study, a hydraulic Reynolds number (Re_h) of 408 is used for all cases under consideration, as it was previously found to be a flow regime that significantly benefits from the synergies between the spacers and unsteady forced slip mass transfer enhancement (Liang et al. 2016). A Helmholtz-Smoluchowski slip velocity ($u_s = -\frac{\varepsilon_e \zeta E_x}{\mu}$) of 0.5 mm s^{-1} with an electric field (E_x) of the order of 10^4 V m^{-1} and a zeta potential (ζ) of the order of -10^{-2} V is used. The slip velocity can be made dimensionless using the fluid density, the hydraulic diameter and the fluid viscosity as $Re_s = \frac{\rho u_{s,A} d_h}{\mu}$. The simulations are restricted to 2D flow because 3D simulations require exponentially higher computational resources and time (especially for transient simulations) than that required to simulate 2D flow. Moreover, since geometries similar to that used here do not present significant 3D effects in the Reynolds number range used for this study (Iwatsu et al. 1989; Reima, Jae Min, and Kunio 1990; Fimbres-Weihs and Wiley 2007), the 3D flow behaviour is not expected to alter the trends in mass transfer behaviour presented in this study.

3.2 Boundary conditions

From the work of Y.Y. Liang et al. (Liang, Fimbres Weihs, and Wiley 2016), only the spacer filament surfaces and the channel walls in the entrance and exit regions are treated as non-slip ($u = v = 0$), while the top and bottom walls of the membrane region have non-zero velocity boundary conditions ($u = u_s$, $v = v_w$ for the top wall and $v = -v_w$ for the bottom wall). The volumetric flux across the membrane (v_w) depends on the local salt concentration, according to the Kedem-Katchalsky-Merten equation (Fane, Wang, and Hu 2015):

$$v_w = \frac{J}{\rho} = L_p(\Delta p_{tm} - \sigma\phi R w_w) \quad 3.4$$

where ρ , σ , ϕ , J , L_p , R , w_w , Δp_{tm} are fluid density, reflection coefficient, osmotic pressure coefficient, permeate flux, membrane permeability, membrane intrinsic rejection, solute concentration fraction at the membrane wall and inlet transmembrane pressure.

The CFD calculation determines the solute concentration at the membrane surface based on a flux balance condition (Fane, Wang, and Hu 2015). A more detailed description of the permeate flux calculation can be found elsewhere (Liang et al. 2014a). The slip velocity is implemented in the form of a sinusoidal waveform, which is defined as (Fimbres-Weihs and Wiley 2010):

$$U_{s,t} = \frac{u_{s,A}}{u_{eff}} \sin(2\pi f_s t) = U_{s,A} \sin(2\pi f_s t) \quad 3.5$$

where t , f_s , u_{eff} and $u_{s,A}$ are time, frequency of oscillation, effective velocity and slip velocity amplitude, respectively.

3.3 Assumption and cases

Around the world, typical concentrations of dissolved solids in brackish water can range from 1,000 to 10,000 mg/L (mass fraction $w = 0.001$ – 0.01), while the typical concentrations for seawater are much higher, ranging from around 35,000 mg/L ($w = 0.035$) to greater than 45,000 mg/L ($w = 0.045$) (Liang et al. 2014a). In this study, we investigate the effect of three different feed solute mass fractions (w_{b0}) under typical conditions for RO, as shown in Table 3.1. For the seawater feed concentration ($w_{b0} =$

0.04), a higher transmembrane pressure is used than for brackish water, in order to achieve a similar permeate flux under higher osmotic pressure.

A mesh independence study was carried out to establish the accuracy of the CFD solution. The final mesh discretisation consists of at least 30 elements within an inflation layer normal to all solid boundaries with a thickness equal to approximately 2 % of the channel height, and non-structured elements with a maximum size of 1 % of the channel height. The mesh used comprised ~2 million elements has a Grid Convergence Index (GCI) below 5 % for both mass transfer and permeate flux, meaning that the mesh resolution is within an acceptable range, and that this potential source of the numerical error can be safely neglected.

3.4 Methodology for analysis of results

Dimensionless variables used in this paper are summarised in Table 3.2.

Table 3.2 Dimensionless variables used for this study

Dimensionless Variable	Definition
Concentration Polarisation Index (γ)	w_w/w_{b0}
Flux (J/J_{pure})	$1 - \gamma\sigma\phi R w_{b0}/\Delta p_{tm}$
Frequency (F_s)	$f_s h_{ch}/u_{eff}$

A method typically used to estimate the peak frequency of a linear dynamic system consists of adding a stimulus to the system and carrying out frequency response analysis (Doebelin 1980). The frequency response is a plot of the amplitude ratio of a system output (e.g. velocity, flux, etc.) for a given input stimulus (e.g. unsteady forced slip). The frequency response plot can be calculated using a stimulus with a broad range of frequencies, such as a pulse, and dividing the Fourier transform of the observed output by the Fourier transform of the stimulus to the system. The peak frequency is the frequency at which the maximum amplitude ratio is observed, and it is termed F_{pl} in this study. However, as the coupled hydrodynamics-mass transfer system in a spacer-filled

channel is strictly non-linear, the peak frequency estimated from frequency response analysis (F_{pl}) is not necessarily the frequency which maximises mass transfer. Nonetheless, in the work by Liang et al. (Liang, Fimbres Weihs, and Wiley 2016) shows that F_{pl} can help approximate the actual peak frequency (F_{peak}) for typical RO operating conditions. Therefore, this study uses frequency response analysis to analyse the effect of membrane permeance on the peak frequency.

The analysis carried out in this study follows the same method as (Liang, Fimbres Weihs, and Wiley 2016), which uses a pulse test to determine the frequency response of v -velocity up until a cut-off frequency (f_{cut}). The input slip velocity in dimensionless form is expressed as:

$$U_{s,pulse} = \begin{cases} 0 & , t < 0, t > t_{fcut} \\ \frac{U_{s,A}}{2} \left[1 - \cos \left(\frac{2\pi t}{t_{fcut}} \right) \right] & , 0 \leq t \leq t_{fcut} \end{cases} \quad 3.6$$

where:

$$t_{fcut} = \frac{4}{\pi f_{cut}} \quad 3.7$$

Pulse tests are carried out using transient simulations, taking as the initial state ($t = 0$), a steady state solution. In addition, transient simulations with a single-frequency sinusoidal slip-velocity input are also carried out.

The time-averaged (ϕ_{TA}) and maximum (ϕ_{max}) values of spatially local variables are recorded after the convergence criteria have been met, that is, after the time-averaged variables have stabilised. The maximum value of wall shear stress ($\bar{\tau}_{max} = \mu \left(\frac{\partial u}{\partial y} \right)_{max}$) is measured because a higher wall shear stress has a greater potential to reduce membrane fouling (Liang et al. 2016). On the other hand, global variables ($\bar{\phi}$) are calculated as the area-average of the local variables along the length (L) of the membrane region of a unit cell (spacer 7 and 8 as indicated in Figure 3.2). Global variables can therefore be expressed by:

$$\bar{\phi} = \frac{1}{L} \int \phi dx \quad 3.8$$

In addition, forced slip mass transfer enhancement is measured by the relative change in the concentration polarisation index (Liang et al. 2014a):

$$\tilde{\Phi} = 1 - \frac{\bar{V}_{EO,TA}}{\bar{V}_{NS}} = \frac{\bar{J}_{EO,TA} - \bar{J}_{NS}}{\bar{J}_{pure} - \bar{J}_{NS}} \quad 3.9$$

Power number ($P_n = Re_h^3 f_{TA}$) is used to measure the energy losses by comparing the pumping power at the same membrane permeance (Fimbres-Weihs and Wiley 2010). Recovery rate is determined by the ratio of the product water flow rate ($Q_p = L_m \bar{J}_{TA} w_{ch}$) to feed water flow rate ($Q_{in} = \rho u_{b0} h_{ch} w_{ch}$) (Baker 2004).

$$Recovery\ rate = \frac{L_m \bar{J}_{TA}}{\rho u_{b0} h_{ch}} \quad 3.10$$

where ρ , h_{ch} , L_m , \bar{J}_{TA} , u_{b0} and w_{ch} are fluid density, height of membrane channel, membrane length, global time-averaged permeate flux, inlet velocity and membrane channel width.

اونيور سیتی ملیسیا قهغ

UNIVERSITI MALAYSIA PAHANG

The flow chart of the overall methodology is described in Figure 3.3

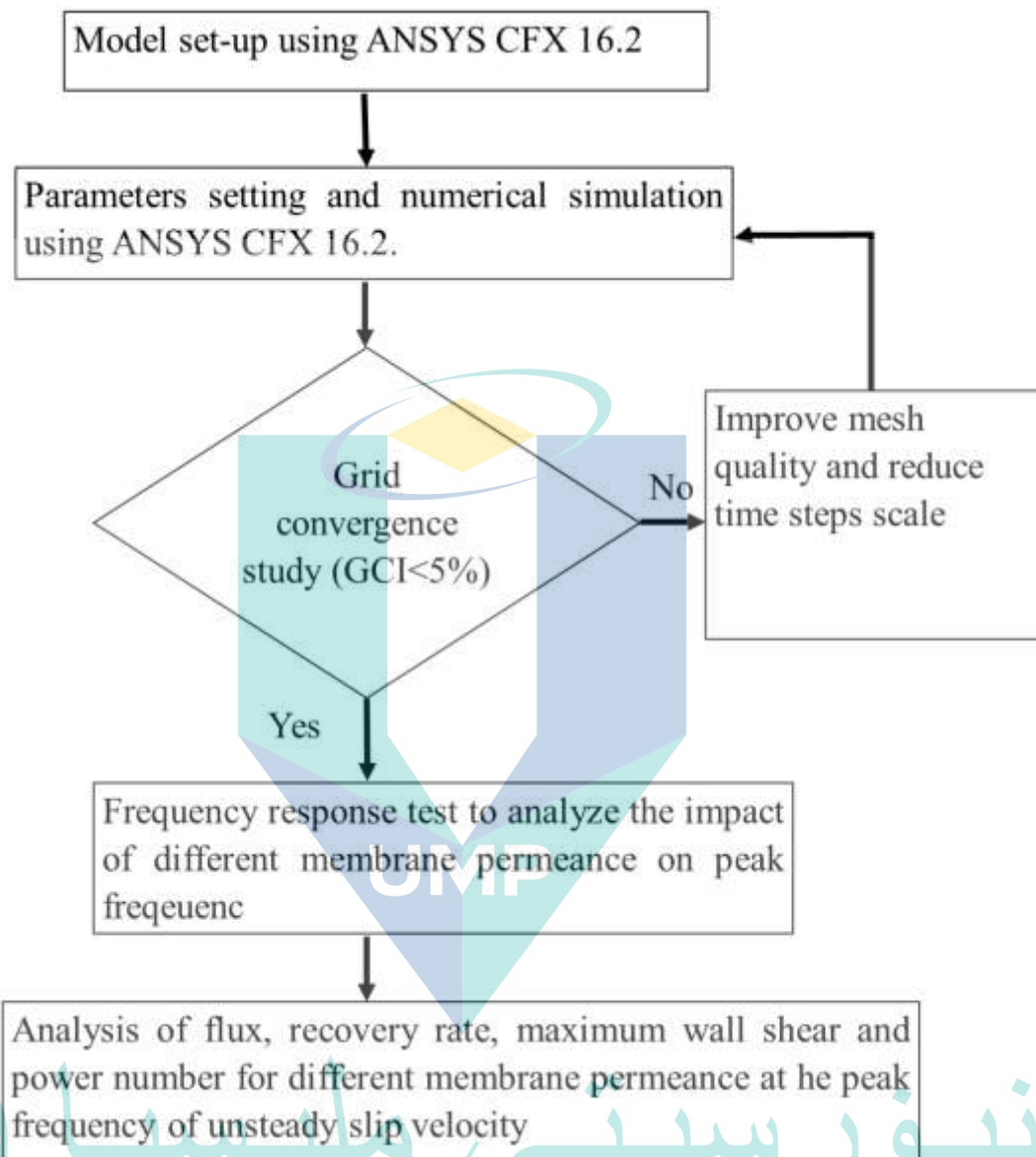


Figure 3.3 Flow chart illustrating the steps taken in this study to carry out numerical study to investigate the effect of membrane permeance on permeate flux enhancement generated by unsteady slip velocity.

CHAPTER 4

RESULTS AND DISCUSSION

The resonant frequency of the forced slip velocity used in this study is determined through a pulse test. The pulse test is carried out using different membrane permeance values with a positive slip velocity for the whole membrane region. The v -velocity is then monitored during the tests at the point ‘•’ as shown in Figure 4.1, the method used here is the same as in the work of Liang et al. (Liang, Fimbres Weihs, and Wiley 2016). It is important to note that the selection of location of monitoring point is not important (Foo, Liang, and Weihs 2020). After a pulse is introduced to the flow, the oscillation of the v -velocity shows a similar pattern and magnitude for each membrane permeance tested. From the work of Liang et al (Liang et al. 2016), it is known that a slip velocity of 1 mm/s has the potential to induce a v -velocity of the order of 30 mm/s for a Reynolds number that is near to the transition from steady to unsteady flow.

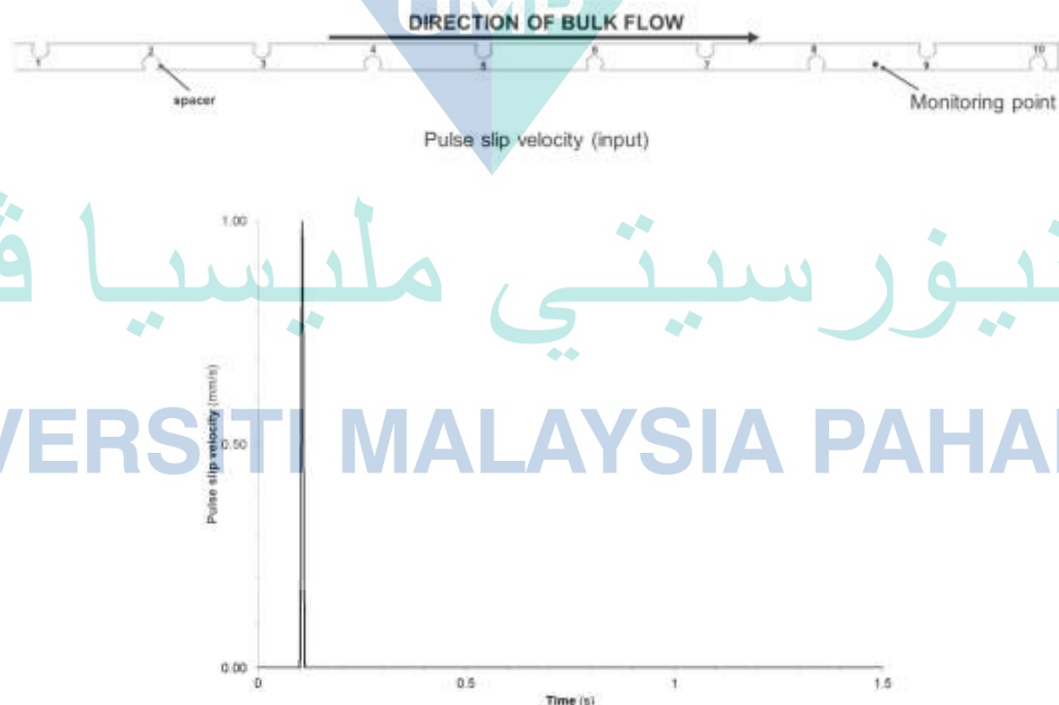
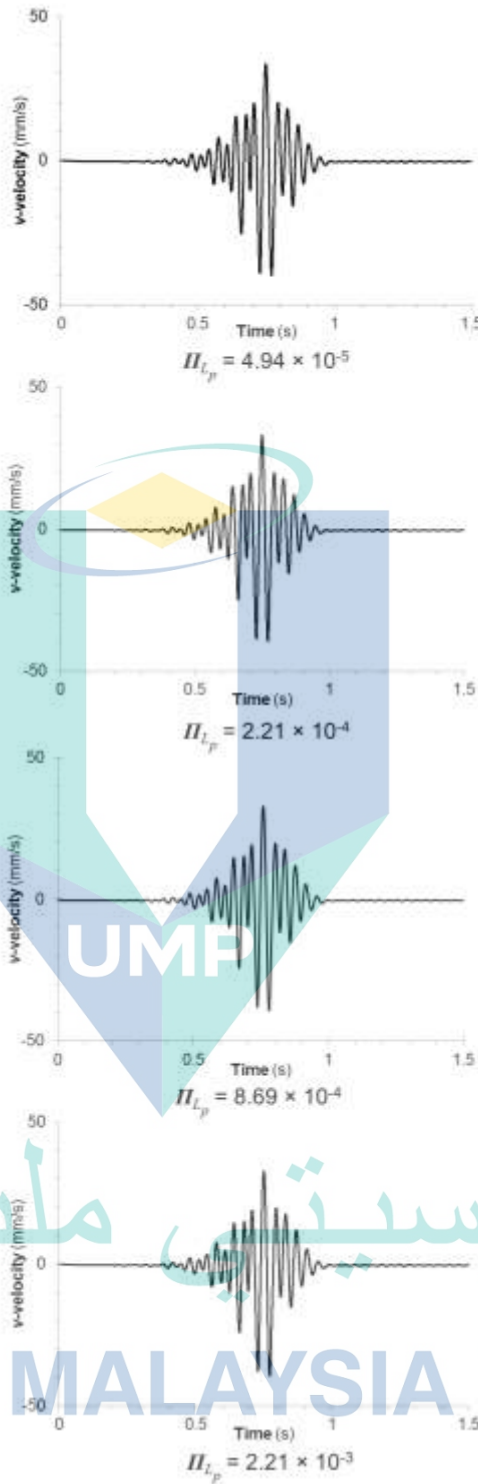


Figure 4.1 Frequency response time data for the pulse slip velocity at monitoring point ‘•’ (located at one third of the channel height from the bottom membrane surface), for $\Pi_{Lp} = 4.94 \times 10^{-5}$, 2.21×10^{-4} , 8.69×10^{-4} and 2.21×10^{-3} at the same feed bulk concentration ($w_{b0} = 0.025$) and $Re = 408$



اونيور سبتى ملايسيا قهق
 UNIVERSITI MALAYSIA PAHANG

Figure 4.2 Frequency response time data for the corresponding v -velocity at monitoring point ‘•’ (located at one third of the channel height from the bottom membrane surface), for $\Pi_{L_p} = 4.94 \times 10^{-5}$, 2.21×10^{-4} , 8.69×10^{-4} and 2.21×10^{-3} at the same feed bulk concentration ($w_{b0} = 0.025$) and $Re = 408$.

Figure 4.3 shows the frequency response obtained from the pulse test in slip velocity (from Figure 4.1 and Figure 4.2). Figure 4.3 also shows similar behaviour (the magnitude of the amplitude ratio and of the peak frequency, $F_{pl} \approx 0.87$) for all of the values of membrane permeance tested. This indicates that the membrane properties and the bulk properties have no significant effect on the peak frequency, this is due to the permeation rate is at least 7,000 times smaller than the bulk flow rate. As the approximate peak frequency of 0.87 determined by the frequency response analysis, as shown in Figure 4.3, is the same as in (Liang, Fimbres Weihs, and Wiley 2016), it is expected that the value of the actual peak frequency ($F_{peak} = 0.67$) determined by a single-frequency sinusoidal slip velocity in (Liang et al. 2014a) is also the same in this study. Therefore, $F_{peak} = 0.67$ is used in this study to examine the effect of membrane permeance on membrane performance enhancement through slip velocity.

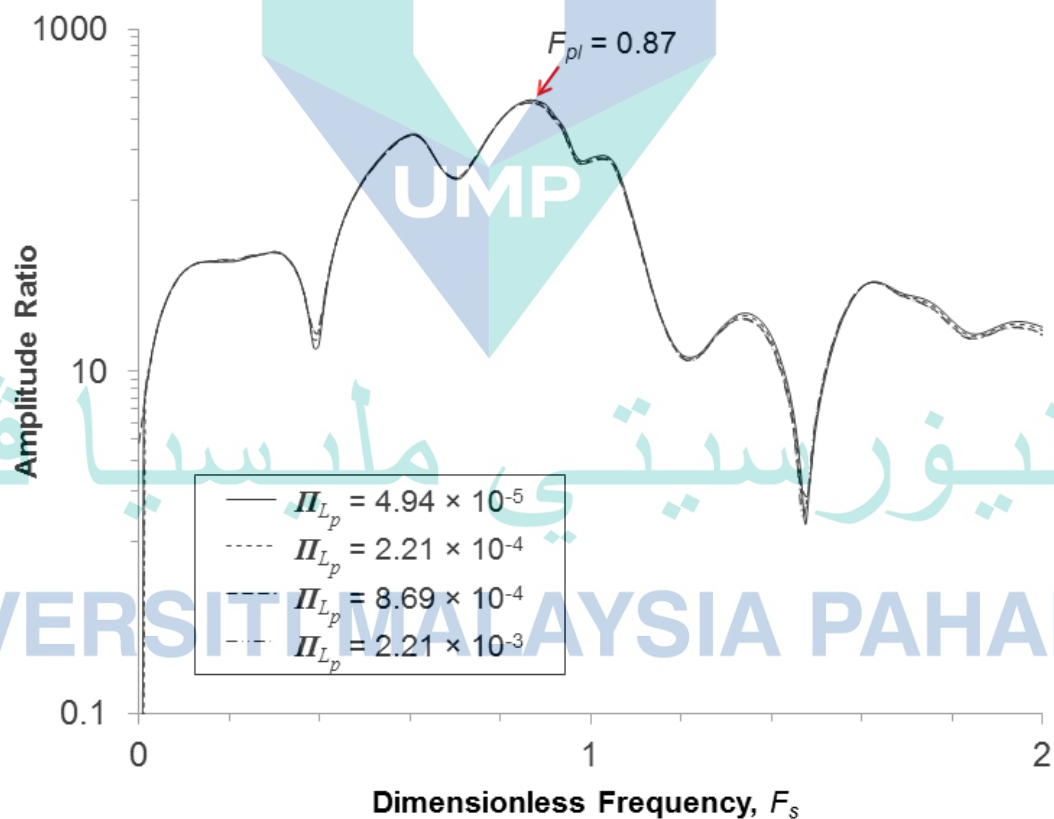


Figure 4.3 Frequency response of v -velocity at location ‘•’ to a pulse in slip velocity for $\Pi_{Lp} = 4.94 \times 10^{-5}$, 2.21×10^{-4} , 8.69×10^{-4} and 2.21×10^{-3} at the same feed solute concentration ($w_{b0} = 0.025$) and $Re = 408$

Figure 4.4 shows the results of simulations that used a forced slip velocity at $F_{peak}=0.67$, and varying the membrane permeance are shown, in terms of mass transfer enhancement ($\tilde{\Phi}$) and flux enhancement (ΔJ). In Figure 4.4a, the forced slip velocity mass transfer enhancement factor ($\tilde{\Phi}$) reaches a maximum at a membrane permeance of $9.87 \times 10^{-12} \text{ m s}^{-1} \text{ Pa}^{-1}$ for all feed bulk concentrations (w_{b0}) tested. The maximum in $\tilde{\Phi}$ indicates that the effectiveness for concentration polarisation reduction is at its best in the mid-range of membrane permeance values typically used for brackish water, and is related to the competing effect between flux ratios ($\bar{J}_{EO}/\bar{J}_{pure}$ and $\bar{J}_{NS}/\bar{J}_{pure}$) in equation 3.9. At a lower membrane permeance, $\tilde{\Phi}$ increases because $\tilde{\Phi}$ is dominated by the difference between $\bar{J}_{EO,TA}$ and \bar{J}_{NS} as the difference between \bar{J}_{pure} and \bar{J}_{NS} is smaller. However, at a higher membrane permeance, $\tilde{\Phi}$ decreases because \bar{J}_{pure} is much larger than \bar{J}_{NS} as both $\bar{J}_{EO,TA}$ and \bar{J}_{NS} approach a constant value. This suggests that at higher feed concentration there is lower flux, which leads to lower concentration polarisation and thus lower mass transfer enhancement. Therefore, at lower CP there is less possibility for further improvement.

Even though Figure 4.4a shows a peak in $\tilde{\Phi}$ at the mid-range brackish water membrane permeance, Figure 4.4b shows that at the high end of membrane permeance tested ($\Pi_{L_p} > 10^{-4}$ or $L_p > 10^{-11} \text{ m s}^{-1} \text{ Pa}^{-1}$), the tendency for forced slip to further increase the permeate flux (and recovery rate) is weaker but does not disappear. This appears to be the case for all w_{b0} values tested. At the largest permeance simulated, the flux was found to increase roughly 23 % due to forced slip, which is significantly higher than the flux increase of around 13 % at the peak in $\tilde{\Phi}$. This is because at a higher permeance, CP is larger and thus the effectiveness of forced slip velocity in enhancing mixing increases, but not at the linear rate at which J_{pure} increases due to a larger L_p . Comparing the effect of permeance on flux enhancement against the results from (Liang, Fimbres Weih, and Wiley 2016), it is clear that steady forced-slip shows less flux enhancement than unsteady forced-slip (about 11 % flux increase at the highest permeance tested, $L_p \sim 3.95 \times 10^{-10} \text{ m s}^{-1} \text{ Pa}^{-1}$). However, the results agree in the sense that a larger increase in permeate flux occurs at a higher membrane permeance despite the decrease in $\tilde{\Phi}$. This means that forced-slip flux enhancement at higher membrane permeance is independent of whether steady or unsteady slip velocity is implemented, and the decrease in $\tilde{\Phi}$ can be explained by the linear increase of J_{pure} as membrane permeance increases.

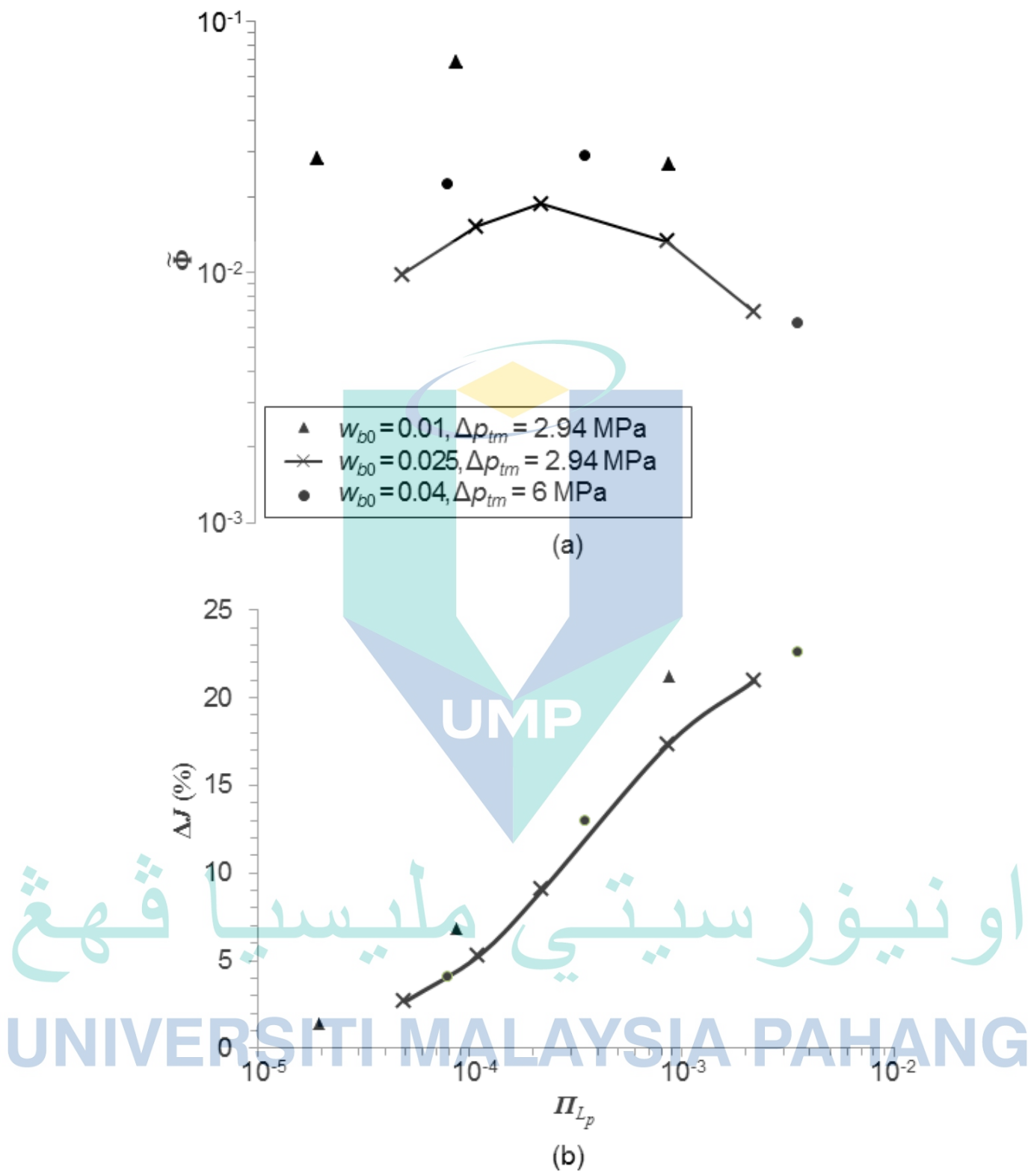


Figure 4.4 Effect of membrane permeance on (a) forced slip velocity mass transfer enhancement and (b) relative change in permeate flux at different inlet solute concentration (w_{b0}) of 0.01 ($\Delta p_{tm} = 2.94 \text{ MPa}$), 0.025 ($\Delta p_{tm} = 2.94 \text{ MPa}$) and 0.04 ($\Delta p_{tm} = 6 \text{ MPa}$) for $Re = 408$.

Figure 4.5 shows the effect of slip velocity applied at F_{peak} on the velocity field and solute concentration, in the region downstream of spacer 8 for the lowest ($\Pi_{L_p} = 4.94 \times 10^{-5}$) and the highest ($\Pi_{L_p} = 2.21 \times 10^{-3}$) membrane permeance values considered. The figure shows that when there is no slip velocity, the solute concentration near the wall for the high end of the membrane permeance ($\Pi_{L_p} = 2.21 \times 10^{-3}$) is significantly larger than that of the low end of the membrane permeance ($\Pi_{L_p} = 4.94 \times 10^{-5}$). However, when a forced slip velocity is applied at the F_{peak} , vortex shedding occurs and there is a similar effect on mass transfer for both high and low end of membrane permeance. This indicates that mass transfer is greatly enhanced by the unsteady effect, particularly due to the occurrence of vortex shedding.

Figure 4.6 shows the results in terms of friction and energy losses for the systems simulated. From Figure 4.6a, it is evident that the forced slip velocity leads to more than a two-fold increase in maximum shear stress ($\bar{\tau}_{max}$) relative to the case without a forced slip velocity, hence indicating the potential for fouling reduction using forced slip. Moreover, membrane permeance has a negligible effect on maximum shear stress under forced slip, with only a 1.8% decrease as permeance increases over 2 orders of magnitude. This slight decrease in maximum shear stress is attributed to the increase in permeate flux as the membrane permeance increases, thus causing a decrease in velocity near the membrane wall. Moreover, Figure 4.6b shows that the pumping energy requirements under forced slip for all L_p and w_{b0} values explored present a slight increase of 5–7 % from the case without forced slip at the same Reynolds number of 408, due to the induction of vortex shedding (Liang, Fimbres Weihs, and Wiley 2016). It should be noted that the energy required to induce vortex shedding depends on the type of flow perturbation approach used.

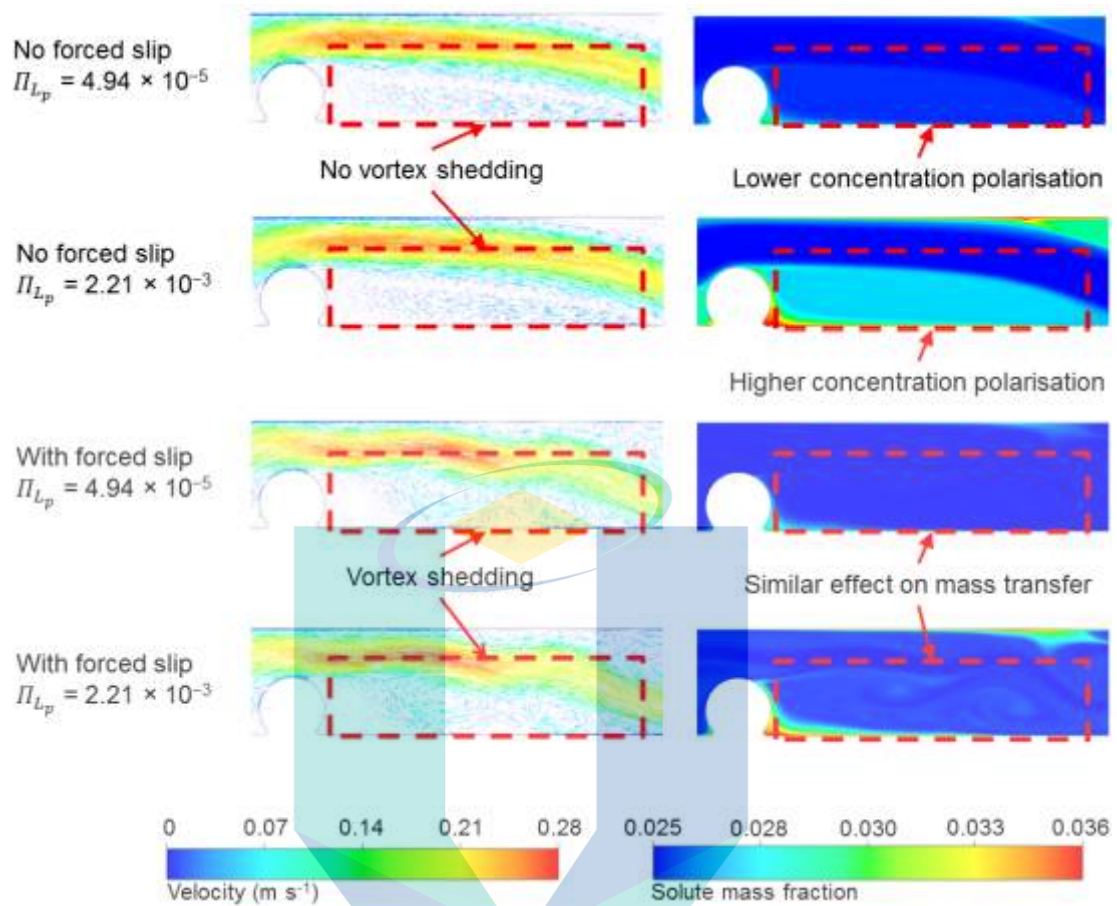


Figure 4.5 Effect of slip velocity applied at the F_{peak} on the velocity field and solute concentration in the region within spacer 8 for $\Pi_{Lp} = 4.94 \times 10^{-5}$ and 2.21×10^{-3} at the same feed solute concentration ($w_{b0} = 0.025$) and $Re = 408$.

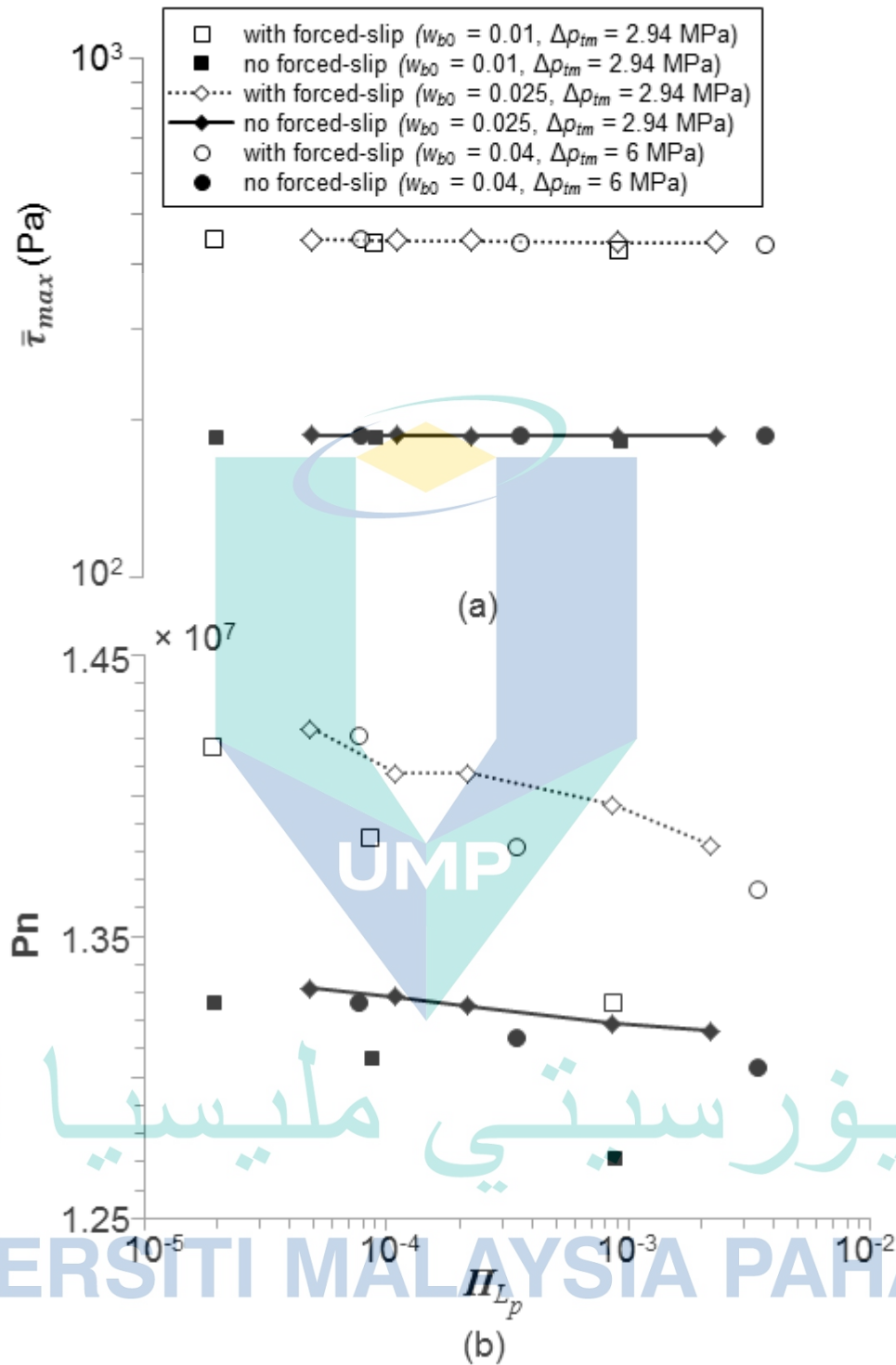


Figure 4.6 Effect of membrane permeance on (a) maximum shear stress and (b) Power number at three different values of w_{b0} : 0.01 ($\Delta p_{tm} = 2.94$ MPa), 0.025 ($\Delta p_{tm} = 2.94$ MPa) and 0.04 ($\Delta p_{tm} = 6$ MPa) for $Re = 408$.

CHAPTER 5

CONCLUSION AND RECOMMENDATIONS

5.1 Conclusions

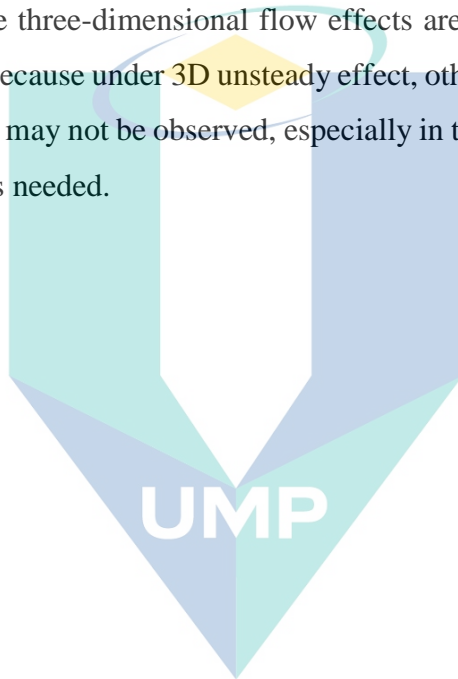
This study investigated the effect of membrane permeance on the resonant frequency, mass transfer and flux enhancement when an unsteady forced slip velocity is applied. The results show that the peak frequency for unsteady forced slip is not significantly affected by the membrane permeance. This is because the magnitude of membrane permeation is not significant when compared with the magnitude of the bulk flow velocity, even at a higher permeance. Although the peak in mass transfer enhancement factor ($\tilde{\Phi}$) indicates that reduction of concentration polarisation is most effective for membrane permeance in the range typically used for brackish water, permeate flux and recovery rate can still be significantly enhanced (by up to 23 %) for higher values of membrane permeance, at the expense of slightly higher (5–7 %) pumping energy requirements. The results also show that at any membrane permeance, forced slip can improve the maximum shear stress ($\bar{\tau}_{max}$) by at least 130 %, thereby reducing the effects of fouling. Overall the results show that forced slip velocity is more effective at a higher operating flux.

Although this study only studies the effect of unsteady forced slip velocity in the vicinity of boundary layer, other hydrodynamic perturbation (forced transients) methods can also be used to affect the flow in the membrane boundary layer and improve mass transfer when applied at the resonant frequency. This is because when a flow perturbation is applied at the resonant frequency, it has the potential to induce vortex shedding which results in a greater mixing and mass transfer enhancement. The results presented in this study suggest that the permeance of typical membranes used for brackish water treatment should not affect the value of the resonant frequency.

5.2 Recommendations

In this study, the effect of membrane permeance on the resonant frequency, mass transfer and flux enhancement is investigated when an unsteady forced slip velocity is applied for only a single type of spacer geometry. As the bulk flow characteristics will likely change for different spacer geometries, it may be possible to further enhance mass transfer if the interaction between the forced slip velocity and the flow induced by different types of spacer geometry is optimised.

In addition, the three-dimensional flow effects are not taken into account in the present work. This is because under 3D unsteady effect, other flow instabilities than those observed for 2D effect may not be observed, especially in the z -direction. Future research in this direction is thus needed.



اونيورسيتي ملايسيا قهغ

UNIVERSITI MALAYSIA PAHANG

REFERENCES

- Abbas, Abderrahim, and Nader Al-Bastaki. 2000. 'Flux enhancement of RO desalination processes', *Desalination*, 132: 21-27.
- Ahmad, A. L., and K. K. Lau. 2006. 'Impact of different spacer filaments geometries on 2D unsteady hydrodynamics and concentration polarization in spiral wound membrane channel', *Journal of Membrane Science*, 286: 77-92.
- Ahmad, A. L., K. K. Lau, M. Z. Abu Bakar, and S. R. Abd Shukor. 2005a. 'Integrated CFD simulation of concentration polarization in narrow membrane channel', *Computers & Chemical Engineering*, 29: 2087-95.
- . 2005b. 'Integrated CFD simulation of concentration polarization in narrow membrane channel', *Computers & Chemical Engineering*, 29: 2087-95.
- Ahmed, Saber, M. G. Rasul, M. A. Hasib, and Y. Watanabe. 2010. 'Performance of nanofiltration membrane in a vibrating module (VSEP-NF) for arsenic removal', *Desalination*, 252: 127-34.
- Akoum, O. Al, Michel Y. Jaffrin, Luhui Ding, Patrick Paullier, and Clotilde Vanhoutte. 2002. 'An hydrodynamic investigation of microfiltration and ultrafiltration in a vibrating membrane module', *Journal of Membrane Science*, 197: 37-52.
- Akoum, Omar, Michel Y. Jaffrin, and Lu-Hui Ding. 2005. 'Concentration of total milk proteins by high shear ultrafiltration in a vibrating membrane module', *Journal of Membrane Science*, 247: 211-20.
- Al-Bastak, Nader M., and Abderrahim Abbas. 1998. 'Periodic Operation of a Reverse Osmosis Water Desalination Unit', *Separation Science and Technology*, 33: 2531-40.
- Al-haj Ali, Mohammad, A. Ajbar, Emadadeen Ali, and K. Alhumaizi. 2011. 'Study of cyclic operation of RO desalination process', *The Canadian Journal of Chemical Engineering*, 89: 299-303.
- . 2013. 'Optimization-based periodic forcing of RO desalination process for improved performance', *Desalination and Water Treatment*, 51: 6961-69.
- Amokrane, M., D. Sadaoui, C. P. Koutsou, A. J. Karabelas, and M. Dudeck. 2015. 'A study of flow field and concentration polarization evolution in membrane channels with two-dimensional spacers during water desalination', *Journal of Membrane Science*, 477: 139-50.
- Baker, R. 2004. *Membrane Technology and Applications* (Wiley).
- Banik, A., T. K. Bandyopadhyay, and S. K. Biswal. 2019. 'Computational Fluid Dynamics (CFD) Simulation of Cross-flow Mode Operation of Membrane for Downstream Processing', *Recent Pat Biotechnol*, 13: 57-68.
- Beier, S. P., and G. Jonsson. 2006. 'Dynamic microfiltration with a vibrating hollow fiber membrane module', *Desalination*, 199: 499-500.

- Beier, Søren Prip, Maria Guerra, Arvid Garde, and Gunnar Jonsson. 2006. 'Dynamic microfiltration with a vibrating hollow fiber membrane module: Filtration of yeast suspensions', *Journal of Membrane Science*, 281: 281-87.
- Brian, P. L. T. 1965. 'Concentration Polarization in Reverse Osmosis Desalination with Variable Flux and Incomplete Salt Rejection', *Industrial & Engineering Chemistry Fundamentals*, 4: 439-45.
- Cohen-Tanugi, David, Ronan K. McGovern, Shreya H. Dave, John H. Lienhard, and Jeffrey C. Grossman. 2014. 'Quantifying the potential of ultra-permeable membranes for water desalination', *Energy & Environmental Science*, 7: 1134-41.
- Culkin, B, and AD Armando. 1992. 'New separation system extends the use of membranes', *Filtration & separation*, 29: 376-78.
- DesalData, Forecast 2015. *DesalData, in, 2015*.
- Doebelin, E.O. 1980. *System Modeling and Response: Theoretical and Experimental Approaches* (Wiley).
- El Kadi, Khadije, Isam Janajreh, and Raed Hashaikeh. 2020. 'Numerical simulation and evaluation of spacer-filled direct contact membrane distillation module', *Applied Water Science*, 10: 174.
- Fane, A. G., R. Wang, and M. X. Hu. 2015. 'Synthetic membranes for water purification: status and future', *Angew Chem Int Ed Engl*, 54: 3368-86.
- Fimbres-Weihs, G A, and D E Wiley. 2007. 'Numerical Study of Mass Transfer in Three-Dimensional Spacer-Filled Narrow Channels with Steady Flow', *Journal of Membrane Science*, 306: 228-43.
- Fimbres-Weihs, G. A., and D. E. Wiley. 2010. 'Review of 3D CFD modeling of flow and mass transfer in narrow spacer-filled channels in membrane modules', *Chemical Engineering and Processing: Process Intensification*, 49: 759-81.
- Fimbres-Weihs, G. A., D. E. Wiley, and D. F. Fletcher. 2006. 'Unsteady Flows with mass transfer in narrow zigzag spacer-filled channels: A numerical study', *Industrial & Engineering Chemistry Research*, 45: 6594-603.
- Fimbres-Weihs, Gustavo Adolfo, and Jesús Álvarez-Sánchez. 2017. 'Synergies Between Pulsatile Flow and Spacer Filaments in Reverse Osmosis Modules.' in Alfredo Maciel-Cerda (ed.), *Membranes: Materials, Simulations, and Applications* (Springer International Publishing: Cham).
- Finnigan, S. M., and J. A. Howell. 1990. 'The effect of pulsed flow on ultrafiltration fluxes in a baffled tubular membrane system', *Desalination*, 79: 181-202.
- Fletcher, D. F., and D. E. Wiley. 2004. 'A computational fluids dynamics study of buoyancy effects in reverse osmosis', *Journal of Membrane Science*, 245: 175-81.

- Foo, K., Y. Y. Liang, and G. A. Fimbres Weihs. 2020. 'CFD study of the effect of SWM feed spacer geometry on mass transfer enhancement driven by forced transient slip velocity', *Journal of Membrane Science*, 597: 117643.
- Genkin, G., T. D. Waite, A. G. Fane, and S. Chang. 2006. 'The effect of vibration and coagulant addition on the filtration performance of submerged hollow fibre membranes', *Journal of Membrane Science*, 281: 726-34.
- Geraldes, Vítor, Viriato Semião, and Maria Norberta de Pinho. 2002. 'The effect of the ladder-type spacers configuration in NF spiral-wound modules on the concentration boundary layers disruption', *Desalination*, 146: 187-94.
- Geraldes, Vítor, Viriato Semiao, and Maria Norberta de Pinho. 2004. 'Concentration polarisation and flow structure within nanofiltration spiral-wound modules with ladder-type spacers', *Computers & Structures*, 82: 1561-68.
- Geraldes, Vitor, Viriato Semião, and Maria Norberta Pinho. 2003. 'Hydrodynamics and concentration polarization in NF/RO spiral-wound modules with ladder-type spacers', *Desalination*, 157: 395-402.
- Gomaa, H. G. 2012. 'Flux characteristics at oscillating membrane equipped with turbulent promoters', *Chemical Engineering Journal*, 191: 541-47.
- Gomaa, H. G., and S. Rao. 2011. 'Analysis of flux enhancement at oscillating flat surface membranes', *Journal of Membrane Science*, 374: 59-66.
- Gomaa, H. G., S. Rao, and M. Al Taweel. 2011. 'Flux enhancement using oscillatory motion and turbulence promoters', *Journal of Membrane Science*, 381: 64-73.
- Gupta, B. B., P. Blanpain, and M. Y. Jaffrin. 1992. 'Permeate flux enhancement by pressure and flow pulsations in microfiltration with mineral membranes', *Journal of Membrane Science*, 70: 257-66.
- Gurreri, L., A. Tamburini, A. Cipollina, G. Micale, and M. Ciofalo. 2016. 'Flow and mass transfer in spacer-filled channels for reverse electrodialysis: a CFD parametrical study', *Journal of Membrane Science*, 497: 300-17.
- Haidari, A. H., S. G. J. Heijman, and W. G. J. van der Meer. 2016. 'Visualization of hydraulic conditions inside the feed channel of Reverse Osmosis: A practical comparison of velocity between empty and spacer-filled channel', *Water Res*, 106: 232-41.
- . 2018. 'Optimal design of spacers in reverse osmosis', *Separation and Purification Technology*, 192: 441-56.
- Hu, Guoqing, and Dongqing Li. 2007. 'Multiscale phenomena in microfluidics and nanofluidics', *Chemical Engineering Science*, 62: 3443-54.
- Huang, Chyohwu, and H. Chen. 2013. 'The Characteristic Analysis of Interrupted Flow Pulsation on Ultrafiltration System', *Applied Mechanics and Materials*, 479-480: 373-79.

- Hunter, R.J. 1981. *Zeta Potential in Colloid Science: Principles and Applications* (Academic Press).
- Ilias, Shamsuddin, and Rakesh Govind. 1990. 'Potential Applications of Pulsed Flow for Minimizing Concentration Polarization in Ultrafiltration', *Separation Science and Technology*, 25: 1307-24.
- Iwatsu, Reima, Katsuya Ishii, Tetuya Kawamura, Kunio Kuwahara, and Jae Min Hyun. 1989. 'Numerical simulation of three-dimensional flow structure in a driven cavity', *Fluid Dynamics Research*, 5: 173-89.
- Jaffrin, Michel Y. 2008. 'Dynamic shear-enhanced membrane filtration: A review of rotating disks, rotating membranes and vibrating systems', *Journal of Membrane Science*, 324: 7-25.
- Jaffrin, Michel Y., Lu-Hui Ding, Omar Akoum, and Ambroise Brou. 2004. 'A hydrodynamic comparison between rotating disk and vibratory dynamic filtration systems', *Journal of Membrane Science*, 242: 155-67.
- Jagannadh, S. Nadh, and H. S. Muralidhara. 1996. 'Electrokinetics methods to control membrane fouling', *Industrial & Engineering Chemistry Research*, 35: 1133-40.
- Johnson, Jon, and Markus Busch. 2012. *Engineering Aspects of Reverse Osmosis Module Design*.
- Keir, Greg, and Veeriah Jegatheesan. 2013. 'A review of computational fluid dynamics applications in pressure-driven membrane filtration', *Reviews in Environmental Science and Bio/Technology*, (in press): doi: 10.1007/s11157-013-9327-x.
- Kennedy, T. J., R. L. Merson, and B. J. McCoy. 1974. 'Improving permeation flux by pulsed reverse osmosis', *Chemical Engineering Science*, 29: 1927-31.
- Kola, Anusha, Yun Ye, Amy Ho, Pierre Le-Clech, and Vicki Chen. 2012. 'Application of low frequency transverse vibration on fouling limitation in submerged hollow fibre membranes', *Journal of Membrane Science*, 409-410: 54-65.
- Kola, Anusha, Yun Ye, Pierre Le-Clech, and Vicki Chen. 2014. 'Transverse vibration as novel membrane fouling mitigation strategy in anaerobic membrane bioreactor applications', *Journal of Membrane Science*, 455: 320-29.
- Kostoglou, Margaritis, and Anastasios J. Karabelas. 2012. 'A mathematical study of the evolution of fouling and operating parameters throughout membrane sheets comprising spiral wound modules', *Chemical Engineering Journal*, 187: 222-31.
- Kraume, M., and A. Drews. 2010. 'Membrane Bioreactors in Waste Water Treatment – Status and Trends', *Chemical Engineering & Technology*, 33: 1251-59.
- La Cerva, Mariagiorgia, Andrea Cipollina, Michele Ciofalo, Mohammed Albeirutty, Nedim Turkmen, Salah Bouguecha, and Giorgio Micale. 2019. 'CFD Investigation of Spacer-Filled Channels for Membrane Distillation', *Membranes*, 9: 91.

- Li, Hong-yu, Christopher D. Bertram, and Dianne E. Wiley. 1998. 'Mechanisms by which pulsatile flow affects cross-flow microfiltration', *AIChE Journal*, 44: 1950-61.
- Li, Tian, Adrian Wing-Keung Law, Merve Cetin, and A. G. Fane. 2013. 'Fouling control of submerged hollow fibre membranes by vibrations', *Journal of Membrane Science*, 427: 230-39.
- Li, Tian, Adrian Wing-Keung Law, and A. G. Fane. 2014. 'Submerged hollow fibre membrane filtration with transverse and longitudinal vibrations', *Journal of Membrane Science*, 455: 83-91.
- Li, Yu-Ling, and Kuo-Lun Tung. 2008. 'The effect of curvature of a spacer-filled channel on fluid flow in spiral-wound membrane modules', *Journal of Membrane Science*, 319: 286-97.
- Li, Yu-Ling, Kuo-Lun Tung, Yu-Shao Chen, and Kuo-Jen Hwang. 2012. 'CFD analysis of the initial stages of particle deposition in spiral-wound membrane modules', *Desalination*, 287: 200-08.
- Liang, Y. Y., M. B. Chapman, G. A. Fimbres Weihs, and D. E. Wiley. 2014a. 'CFD modelling of electro-osmotic permeate flux enhancement on the feed side of a membrane module', *Journal of Membrane Science*, 470: 378-88.
- . 2014b. 'CFD modelling of electro-osmotic permeate flux enhancement on the feed side of a membrane module', *Journal of Membrane Science*, 470: 378-88.
- Liang, Y. Y., G. A. Fimbres Weihs, and D. E. Wiley. 2014a. 'Approximation for modelling electro-osmotic mixing in the boundary layer of membrane systems', *Journal of Membrane Science*, 450: 18-27.
- . 2014b. 'Approximation for modelling electro-osmotic mixing in the boundary layer of membrane systems', *Journal of Membrane Science*, 450: 18-27.
- . 2016. 'CFD modelling of electro-osmotic permeate flux enhancement in spacer-filled membrane channels', *Journal of Membrane Science*, 507: 107-18.
- . 2020. 'Comparison of oscillating flow and slip velocity mass transfer enhancement in spacer-filled membrane channels: CFD analysis and validation', *Journal of Membrane Science*, 593: 117433.
- Liang, Yong Yeow, Gustavo Fimbres Weihs, Ridwan Setiawan, and Dianne Wiley. 2016. 'CFD modelling of unsteady electro-osmotic permeate flux enhancement in membrane systems', *Chemical Engineering Science*, 146: 189-98.
- Low, S. C., W. X. Jin, and Michael Tan. 2004. 'Characteristics of particle and membrane pore sizes in the performance of water recovery from a fine carbon loaded wastewater using a vibration membrane system', *Desalination*, 167: 217-26.
- Low, S. C., Han Hee Juan, and Low Kwok Siang. 2005. 'A combined VSEP and membrane bioreactor system', *Desalination*, 183: 353-62.

- Ma, Shengwei, and Lianfa Song. 2006. 'Numerical study on permeate flux enhancement by spacers in a crossflow reverse osmosis channel', *Journal of Membrane Science*, 284: 102-09.
- Ma, Shengwei, Lianfa Song, Say-Leong Ong, and Jern Ng. 2004. *A 2-D streamline upwind Petrov/Galerkin finite element model for concentration polarization in spiral wound reverse osmosis modules.*
- Matthiasson, Einar, and Björn Sivik. 1980. 'Concentration polarization and fouling', *Desalination*, 35: 59-103.
- Oberkampf, William L., and Timothy G. Trucano. 2002. 'Verification and validation in computational fluid dynamics', *Progress in Aerospace Sciences*, 38: 209-72.
- Parvareh, A., M. Rahimi, S. S. Madaeni, and A. A. Alsairafi. 2011. 'Experimental and CFD Study on the Role of Fluid Flow Pattern on Membrane Permeate Flux', *Chinese Journal of Chemical Engineering*, 19: 18-25.
- Patankar, Neelesh A., and Howard H. Hu. 1998. 'Numerical Simulation of Electroosmotic Flow', *Analytical Chemistry*, 70: 1870-81.
- Pawlowski, Sylwin, Vítor Geraldés, João G. Crespo, and Svetlozar Velizarov. 2016. 'Computational fluid dynamics (CFD) assisted analysis of profiled membranes performance in reverse electrodialysis', *Journal of Membrane Science*, 502: 179-90.
- Petala, M. D., and A. I. Zouboulis. 2006. 'Vibratory shear enhanced processing membrane filtration applied for the removal of natural organic matter from surface waters', *Journal of Membrane Science*, 269: 1-14.
- Postlethwaite, J., S. R. Lamping, G. C. Leach, M. F. Hurwitz, and G. J. Lye. 2004. 'Flux and transmission characteristics of a vibrating microfiltration system operated at high biomass loading', *Journal of Membrane Science*, 228: 89-101.
- Prip Beier, Søren, and Gunnar Jonsson. 2009. 'A vibrating membrane bioreactor (VMBR): Macromolecular transmission—influence of extracellular polymeric substances', *Chemical Engineering Science*, 64: 1436-44.
- Probstein, R.F. 1989. *Physicochemical hydrodynamics: An Introduction* (Butterworths).
- Rawool, A., and Sushanta Mitra. 2006. 'Numerical simulation of electroosmotic effect in serpentine channels', *Microfluidics and Nanofluidics*, 2: 261-69.
- Reima, Iwatsu, Hyun Jae Min, and Kuwahara Kunio. 1990. 'Analyses of three-dimensional flow calculations in a driven cavity', *Fluid Dynamics Research*, 6: 91-102.
- Roache, P. J. 1997. 'Quantification of uncertainty in computational fluid dynamics', *Annual Review of Fluid Mechanics*, 29: 123-60.
- Roache, Patrick J., and Patrick M. Knupp. 1993. 'Completed Richardson extrapolation', *Communications in Numerical Methods in Engineering*, 9: 365-74.

- Rodrigues, Carina, Vítor Geraldês, Maria Norberta de Pinho, and Viriato Semião. 2012. 'Mass-transfer entrance effects in narrow rectangular channels with ribbed walls or mesh-type spacers', *Chemical Engineering Science*, 78: 38-45.
- Russel, W.B., D.A. Saville, and W.R. Schowalter. 1992. *Colloidal Dispersions* (Cambridge University Press).
- Saremirad, Pegah, Hassan Goma, and Jesse Zhu. 2012. 'Effect of flow oscillations on mass transfer in electrodialysis with bipolar membrane', *Journal of Membrane Science*, s 405–406: 158–66.
- Schlesinger, S. 1979. 'Terminology for model credibility', *SIMULATION*, 32: 103-04.
- Schwinge, J., P. R. Neal, D. E. Wiley, D. F. Fletcher, and A. G. Fane. 2004. 'Spiral wound modules and spacers: Review and analysis', *Journal of Membrane Science*, 242: 129-53.
- Schwinge, J., D. E. Wiley, and A. G. Fane. 2004. 'Novel spacer design improves observed flux', *Journal of Membrane Science*, 229: 53-61.
- Schwinge, J., D. E. Wiley, A. G. Fane, and R. Guenther. 2000. 'Characterization of a zigzag spacer for ultrafiltration', *Journal of Membrane Science*, 172: 19-31.
- Schwinge, J., D. E. Wiley, and D. F. Fletcher. 2002. 'Simulation of the flow around spacer filaments between narrow channel walls. 1. Hydrodynamics', *Industrial & Engineering Chemistry Research*, 41: 2977-87.
- Shaw, R. A., R. Deluca, and William N. Gill. 1972. 'Reverse osmosis: increased productivity by reduction of concentration polarization in laminar flow reverse osmosis using intermediate non-rejecting membrane sections', *Desalination*, 11: 189-205.
- Sherwood, T. K., P. L. T. Brian, R. E. Fisher, and Lawrence Dresner. 1965. 'Salt Concentration at Phase Boundaries in Desalination by Reverse Osmosis', *Industrial & Engineering Chemistry Fundamentals*, 4: 113-18.
- Shi, Wei, and Mark M. Benjamin. 2011. 'Effect of shear rate on fouling in a Vibratory Shear Enhanced Processing (VSEP) RO system', *Journal of Membrane Science*, 366: 148-57.
- Su, Xu, Wende Li, Alan Palazzolo, and Shehab Ahmed. 2019. 'Permeate flux increase by colloidal fouling control in a vibration enhanced reverse osmosis membrane desalination system', *Desalination*, 453: 22-36.
- Suresh, K., K. Selvam, and B. Karunanithi. 2019. 'CFD simulation studies on the flow behavior of power-law fluids used to extrude the polymeric hollow fiber membrane through an angular spinneret', *AIP Conference Proceedings*, 2112: 020160.
- Thomas, Aaron, and Aashika Jain. 2007. 'The Effect of Pulsatile Flows on the Transport Across Membranes: An Analytical and Experimental Study', *Separation Science and Technology*, 42: 1931-44.

- Vrouwenvelder, J. S., C. Picioreanu, J. C. Kruithof, and M. C. M. van Loosdrecht. 2010. 'Biofouling in spiral wound membrane systems: Three-dimensional CFD model based evaluation of experimental data', *Journal of Membrane Science*, 346: 71-85.
- Wardeh, S., and H. P. Morvan. 2008. 'CFD simulations of flow and concentration polarization in spacer-filled channels for application to water desalination', *Chemical Engineering Research and Design*, 86: 1107-16.
- Wiley, Dianne E., and David F. Fletcher. 2003. 'Techniques for computational fluid dynamics modelling of flow in membrane channels', *Journal of Membrane Science*, 211: 127-37.
- Winzeler, Heinz B., and Georges Belfort. 1993. 'Enhanced performance for pressure-driven membrane processes: the argument for fluid instabilities', *Journal of Membrane Science*, 80: 35-47.
- Yang, Xing, Hui Yu, Rong Wang, and Anthony G. Fane. 2012. 'Analysis of the effect of turbulence promoters in hollow fiber membrane distillation modules by computational fluid dynamic (CFD) simulations', *Journal of Membrane Science*, 415-416: 758-69.
- Zamani, Farhad, Jia Wei Chew, Ebrahim Akhondi, William B. Krantz, and Anthony G. Fane. 2015. 'Unsteady-state shear strategies to enhance mass-transfer for the implementation of ultrapermeable membranes in reverse osmosis: A review', *Desalination*, 356: 328-48.
- Zouboulis, A. I., and M. D. Petala. 2008. 'Performance of VSEP vibratory membrane filtration system during the treatment of landfill leachates', *Desalination*, 222: 165-75.

اونيورسيتي ملايسيا قهغ

UNIVERSITI MALAYSIA PAHANG